The insulin receptor adaptor IRS2 is an APC/C substrate that promotes cell cycle protein expression and a robust spindle assembly checkpoint

Sandhya Manohar[1], Qing Yu[1], Steven P. Gygi[1], Randall W. King[1,2*]

1. Department of Cell Biology, Harvard Medical School, Boston, Massachusetts 02115, USA.
2. Lead contact

* Correspondence: randy_king@hms.harvard.edu

Abstract

Insulin receptor substrate 2 (IRS2) is an essential adaptor that mediates signaling downstream of the insulin receptor and other receptor tyrosine kinases. Transduction through IRS2-dependent pathways is important for coordinating metabolic homeostasis, and dysregulation of IRS2 causes systemic insulin signaling defects. Despite the importance of maintaining proper IRS2 abundance, little is known about what factors mediate its protein stability. We conducted an unbiased proteomic screen to uncover novel substrates of the Anaphase Promoting Complex/Cyclosome (APC/C), a ubiquitin ligase that controls the abundance of key cell cycle regulators. We found that IRS2 levels are regulated by APC/C activity and that IRS2 is a direct APC/C target in G_1. Consistent with the APC/C's role in degrading cell cycle regulators, quantitative proteomic analysis of IRS2-null cells revealed a deficiency in proteins involved in cell cycle progression. We further show that cells lacking IRS2 display a weakened spindle assembly checkpoint in cells treated with microtubule inhibitors. Together, these findings reveal a new pathway for IRS2 turnover and indicate that IRS2 is a component of the cell cycle control system in addition to acting as an essential metabolic regulator.

Keywords

Anaphase-Promoting Complex/Cyclosome; ubiquitin; cell cycle; insulin signaling pathway; G_1

Introduction

The insulin and insulin-like growth factor 1 receptors (IR/IGF1R) are receptor tyrosine kinases that control metabolism, differentiation, and growth. Upon ligand binding at the cell surface, the activated IR/IGF1R undergoes a conformational change that allows it to auto-phosphorylate tyrosine residues on its cytoplasmic subunits [1]. This facilitates the recruitment and phosphorylation of insulin receptor substrate (IRS) proteins, which serve as scaffolds to initiate downstream signaling [2]. Two major pathways that are stimulated by this cascade are the PI3K-AKT and Ras-Raf-MAPK pathways, which coordinate metabolic homeostasis and growth, among other functions [1].

The most physiologically important and ubiquitously expressed IRS proteins are IRS1 and IRS2. Though IRS1 and IRS2 share similar structural and functional features, they have complementary roles and expression patterns that depend on tissue type and physiological state [1]. These differences are illustrated by divergent phenotypes in knockout mice: whereas IRS1 knockout mice exhibit insulin resistance that is compensated by increased pancreatic β cell mass, IRS2 knockout mice exhibit β cell failure and resultant diabetes [3]. Distinct roles for IRS1 and IRS2 can also be observed within the same tissue. For example, in skeletal muscle, IRS1 is required for glucose uptake and metabolism, whereas IRS2 is important for lipid uptake and metabolism [4, 5]. Furthermore, recent work has shown that the ratio of IRS1 to IRS2 is important for hepatic glucose metabolism [6]. Thus, maintaining proper IRS1 and IRS2 levels is critical for systemic and cellular homeostasis.

The ubiquitin-mediated proteolysis of IRS proteins is important for restraining signaling through the IR/IGF1R. For example, both IRS proteins are targeted for proteasomal destruction following persistent insulin or IGF1 stimulation in a negative feedback loop that attenuates PI3K-AKT signaling [2, 7]. In mice, removal of a ubiquitin ligase that is responsible for IGF1-induced degradation of IRS1 enhances insulin sensitivity and increases plasma glucose clearance [7]. Though several ubiquitin ligases have been reported to control IRS1's proteasome-dependent degradation [8-12], only SOCS1/3 have been implicated in driving IRS2 turnover [11]. This is an intriguing disparity because hepatic IRS1 remains stable between fasting and feeding whereas IRS2 levels drop after feeding [13], suggesting that IRS2 is less stable than IRS1 in some

63 physiological contexts. Because SOCS1/3 also targets IRS1, there are no reports of
64 ubiquitin ligases that target IRS2 but not IRS1, leaving a gap in our knowledge of how
65 IRS1 and IRS2 are differentially regulated by the ubiquitin proteasome system.

66 The Anaphase-Promoting Complex/Cyclosome (APC/C) is a 1.2 mDa ubiquitin
67 ligase that targets key cell cycle related proteins for destruction by the proteasome [14,
68 15]. To transfer ubiquitin to its substrates, the APC/C works with one of two co-activators:
69 Cdc20 during M-phase or Cdh1 during G_1. These co-activators stimulate the catalytic
70 activity of the APC/C and facilitate substrate recognition. APC/C^{Cdc20} and APC/C^{Cdh1}
71 recognize substrates via short degron motifs in unstructured protein regions called
72 destruction boxes (D-boxes) and KEN-boxes. An additional degron, called the ABBA
73 motif, is used only used by APC/C^{Cdc20} in metazoan cells [14-16].

74 To probe the substrate landscape of the APC/C, we conducted an unbiased
75 proteomic screen by acutely blocking APC/C^{Cdh1} activity with small molecule APC/C
76 inhibitors (apcin and proTAME) [17, 18] in G_1 cells. Using this approach, we uncovered
77 diverse putative APC/C^{Cdh1} substrates, including IRS2. We demonstrate that IRS2, but
78 not IRS1, is a direct target of APC/C^{Cdh1}, thereby establishing a novel mode by which
79 IRS1 and IRS2 are differentially regulated. Using IRS2 knockout cell lines, we show that
80 IRS2 is important for the expression of proteins involved in cell cycle progression. We
81 further show that genetic deletion of IRS2 perturbs spindle assembly checkpoint function.
82 Taken together, these data establish a role for IRS2 in normal cell cycle progression,
83 revealing new connections between an essential component of the growth factor signaling
84 network and cell cycle regulation.

85

86 **Results**

87 *Chemical proteomics reveals proteins whose abundances are APC/C^{Cdh1} regulated*

88 To identify novel substrates and pathways regulated by APC/C^{Cdh1}, we designed
89 an experiment that coupled small molecule inhibition of the APC/C in G_1 cells to high
90 resolution tandem mass tag (TMT)-based quantitative proteomics (**Figure 1A**). Blocking
91 Cdk4/6 activity inhibits Rb phosphorylation, causing cells to arrest at the G_1 restriction
92 point [19]. Thus, to generate a homogeneous population of G_1 cells, we treated
93 asynchronous hTERT-RPE1 cells bearing fluorescent ubiquitination-based cell cycle

94 indicator (FUCCI) constructs [20] with the Cdk4/6 inhibitor palbociclib. Following G_1
95 arrest, cells were acutely treated with a combination of APC/C inhibitors (6 μM proTAME
96 + 50 μM apcin) or vehicle (DMSO) for 8 hours. Cells were then collected for proteomic
97 analysis with the expectation that APC/C-regulated proteins would be stabilized in cells
98 treated with APC/C inhibitors compared to control cells (**Figure 1A**). The combined use
99 of proTAME and apcin results in robust inhibition of the APC/C [17], which guided our
100 decision to use this treatment scheme. Moreover, this scheme was designed to
101 specifically identify APC/C^{Cdh1} substrates rather than APC/C^{Cdc20} substrates since
102 APC/C^{Cdh1} degrades Cdc20 during G_1 phase [21]. Illustrating this point, Cdc20 expression
103 was strongly reduced in G_1 palbociclib-arrested cells (**Figure 1B**). The expression of
104 cyclins A and B was also reduced, consistent with a G_1 block.

105 The experimental approach outlined in **Figure 1A** was validated using the FUCCI
106 reporter system. This system relies on the expression of two stably integrated fluorescent
107 fusion proteins—mAG1-geminin (1-110) and mCherry-Cdt1 (30-120)—to monitor the
108 activity of endogenous cell cycle-related ubiquitin ligases APC/C^{Cdh1} and SCF^{Skp2},
109 respectively [20]. As expected, cells treated with palbociclib showed a reduction in mAG1-
110 geminin (1-110) fluorescence over time due to APC/C^{Cdh1} activity while mCherry-Cdt1
111 (30-120) intensity was increased, indicating G_1 arrest (**Figures S1A-S1B**). The addition
112 of APC/C inhibitors in palbociclib-arrested cells rescued mAG1-geminin (1-110) levels
113 (**Figures S1C-S1D**), confirming that this workflow stabilizes APC/C targets. Notably, cells
114 released from palbociclib-mediated arrest accumulate mAG1-geminin (1-110) more
115 rapidly than palbociclib-arrested cells treated with APC/C inhibitors (**Figure S1E**),
116 indicating that APC/C inhibition is likely insufficient to trigger cell cycle re-entry under
117 these conditions.

118 Using TMT-coupled quantitative proteomics, we identified and quantified relative
119 abundances for ~8000 human proteins in G_1-arrested cells treated with or without APC/C
120 inhibitors in biological triplicate (**Supplementary Table S1**). Notably, we detected 38
121 previously reported APC/C substrates in our dataset (**Figures 1C-1E; Supplementary**
122 **Table S2).** Of these, 22 increased significantly ($p < 0.05$) under conditions of APC/C
123 inhibition. We validated these findings in the context of several previously reported
124 substrates by immunoblot (**Figure 1D**). As an internal control, we detected a significant

125 increase (p = 3.2 x 10^{-5}) in the abundance of peptides derived from the N-terminal 110
126 amino acids of geminin (GMNN). These residues are shared with the mAG1-geminin (1-
127 110) reporter expressed in this cell line, confirming earlier fluorescence-based validation
128 of our experimental system.

129 While the majority of the previously reported APC/C^{Cdh1} substrates that were
130 quantified in our G_1 proteomic experiment were stabilized following APC/C inhibition,
131 some remained constant. There are several possible explanations for this result. First, for
132 proteins that were identified based on few peptides, inadequate quantification may have
133 resulted in inaccurate abundance assignments. Second, some substrates may be
134 APC/C^{Cdh1}-accessible only under conditions or in tissue types that were not met by the
135 experimental parameters that we used. Third, some proteins (e.g. FBXW5, ZC3HC1) [22,
136 23] were proposed to be APC/C^{Cdh1} substrates based on results obtained in Cdh1
137 overexpression systems, indicating that APC/C^{Cdh1} activity may be sufficient but not
138 necessary to control their levels.

139 Of the 38 previously reported APC/C substrates that we identified, the median fold
140 change under APC/C inhibition compared to DMSO was 1.15. Based on this, to identify
141 new APC/C substrates, we screened for proteins that: (1) had a fold change ≥1.15 under
142 APC/C inhibition, (2) were identified and quantified based on >1 peptide, and (3) had a p-
143 value < 0.05 across the three biological replicates measured in this experiment. This
144 narrowed our analysis to a subset of 204 proteins (**Supplementary Table S3**). Because
145 the APC/C recognizes substrates based on D-box motifs (RxxL or the extended motif
146 RxxLxxxxN) and KEN-box motifs (KEN), we used the SLiMSearch (Short Linear Motif
147 Search) degron prediction tool [16, 24] to scan this 204-protein subset for proteins that
148 contain these sequences. In order to classify a putative D- or KEN-box sequence as a
149 probable physiological degron, we applied the following restrictions on the SLiMSearch
150 [24] parameters: (1) similarity score ≥ 0.75; (2) consensus similarity is medium or high;
151 (3) disorder score ≥ 0.4; (4) the putative degron must be intracellular and exist on a non-
152 secreted protein. These cutoffs were determined based on those met by previously
153 validated APC/C substrates (including those not identified in our dataset) and by the
154 physical restriction that APC/C activity occurs within the cell. Based on these thresholds,
155 our analysis identified 26 proteins as potential D- and KEN-box containing APC/C^{Cdh1}

156 substrates (**Table 1, Figure 1E**). Of these 26 proteins, 11 have previously been reported
157 as direct APC/C substrates, validating internally that this analysis was useful for
158 identifying APC/C substrates.
159
160 *IRS2 levels are controlled by Cdh1 in a proteasome-dependent manner*
161 Examining our 26-protein putative substrate list, we focused our attention on
162 IRS2—one of two major adaptors that promotes signaling through the insulin and insulin-
163 like growth factor 1 receptors (IR/IGF1R). Using conditions identical to those under which
164 the proteomics experiment was conducted, we validated that IRS2 was upregulated at
165 the protein level under APC/C inhibition in G_1-arrested RPE1 cells by immunoblot (**Figure**
166 **2A**). Seeking to further validate this result in a distinct physiological context, we asked
167 whether APC/C inhibition in terminally differentiated C_2C_{12} myotubes also increases IRS2
168 protein abundance. C_2C_{12} myoblasts easily differentiate into multinucleated myotubes
169 following serum withdrawal and supplementation with growth factors (**Figures S2A-S2B**).
170 To validate that the APC/C is active in this system, we transfected C_2C_{12} myoblasts with
171 a model APC/C substrate (N-terminal fragment of cyclin B1 fused to EGFP; NT-CycB-
172 GFP), allowed cells to differentiate into myotubes, and found that APC/C inhibition
173 stabilized NT-CycB-GFP (**Figure S2C**). Similarly, we found that acute APC/C inhibition in
174 myotubes also resulted in an accumulation of IRS2 protein (**Figure 2B**), thereby validating
175 this finding from our G_1 experiment in RPE1 cells in an independent system.
176 To exclude the possibility that the change in IRS2 abundance that we observed
177 following APC/C inhibition was due to off-target effects of the small molecule APC/C
178 inhibitors, we depleted Cdh1 using RNAi to block APC/C^{Cdh1} activity in HeLa, RPE1, and
179 asynchronous C_2C_{12} cells (**Figure 2C-2D**, **Figure S2D**). We found that Cdh1 knockdown
180 caused an accumulation of endogenous IRS2 as well as several other previously reported
181 APC/C substrates compared to control-transfected cells (**Figure 2C-2D**).
182 To address whether increased APC/C^{Cdh1} activity is sufficient to reduce IRS2
183 levels, we overexpressed myc-tagged human Cdh1 in HeLa cells. We found that, when
184 expressed at sufficiently high levels, Cdh1 reduced the levels of both IRS2 as well as
185 other known APC/C^{Cdh1} substrates including anillin, TK1, and Top2a (**Figure 2E**) [25-27].
186 The requirement that Cdh1 be expressed at high levels to observe this effect is likely due

187 to Cdk-dependent inhibitory phosphorylation of Cdh1 limiting its ability to activate APC/C
188 under sub-saturating conditions [28].
189 We next sought to confirm that the increase in IRS2 protein observed under APC/C
190 inhibition was due to impaired targeting of IRS2 to the proteasome. To test this, we
191 arrested RPE1 cells in G_1 using palbociclib and acutely treated them with APC/C inhibitors
192 and/or a proteasome inhibitor (MG132) for 8 hours. This experiment revealed that APC/C
193 inhibition or proteasome inhibition each resulted in an accumulation of IRS2 (**Figure 2F**).
194 Notably, co-inhibition of the APC/C and the proteasome did not result in additional
195 stabilization of IRS2, indicating that the increase in IRS2 we observed under APC/C
196 inhibition was solely a consequence of its impaired proteasomal degradation. Consistent
197 with this observation, we found that APC/C inhibition decreased the polyubiquitination of
198 HA-tagged IRS2 in HeLa cells treated with MG132 (**Figure 2G**).
199
200 *IRS2 levels and phosphorylation fluctuate in a cell-cycle dependent manner*
201 To test whether IRS2 levels fluctuate during the cell cycle as expected for an
202 APC/C substrate, we synchronized HeLa cells in early S-phase by double thymidine block
203 and tracked IRS2 protein abundance leading into mitotic entry by immunoblot (**Figure**
204 **3A**). As is typical for APC/C substrates, IRS2 levels correlated with cyclin B1 abundance
205 and APC3 phosphorylation. To assess IRS2 levels at mitotic exit, we thymidine-
206 nocodazole synchronized HeLa cells, released them into prometaphase, and tracked
207 IRS2's abundance through mitotic exit (**Figure 3B**). Again, IRS2 protein abundance
208 correlated with cyclin B1 levels and APC3 phosphorylation. The same behavior was
209 observed in RPE1 cells that were synchronized in late G_2 by RO3306 treatment (Cdk1
210 inhibition) and tracked over the course of progression through M-phase and into G_1
211 (**Figure 3C**). Based on these data, we conclude that IRS2 protein levels fluctuate in a cell
212 cycle-dependent manner that is consistent with other known APC/C substrates. This
213 behavior is also consistent with IRS2 being a potential APC/C^{Cdc20} substrate.
214 In agreement with previous reports of mitotic phosphorylation of IRS2 by Plk1 [29],
215 our cell cycle analysis experiments revealed that IRS2 displays a marked electrophoretic
216 mobility shift consistent with mitotic phosphorylation. This may owe, at least in part, to
217 Cdk1 activity given that HeLa cells released from a double thymidine block into Cdk1

218 inhibitor RO3306 did not display an observable shift in IRS2 mobility as compared to
219 those released into control (DMSO) treatment (**Figure S3**). IRS2 abundance still peaked
220 normally at this time point in the presence of RO3306, suggesting that the increase in
221 IRS2 abundance was not dependent on Cdk1 activity. Together, these results support
222 previous findings [29] that IRS2 is subject to cell-cycle dependent phosphorylation and
223 that its abundance peaks in M-phase and falls in early G_1 in multiple cell lines.
224
225 *Cdh1 control of IRS2 degradation depends on an IRS2 D-box motif*
226 Using the SLiMSearch analysis tool [16], we found that IRS2 contains four minimal
227 D-box motifs (RxxL), one extended D-box motif (RxxLxxxxN) and no KEN-box motifs. Of
228 the four minimal D-box motifs, none bears strong consensus similarity to previously
229 validated D-box motifs, and one exists in a highly structured region of the protein [24].
230 Because of its high SLiMSearch parameter scores (**Table 1**), we focused our efforts on
231 determining whether the extended D-box motif located in the C-terminal third of IRS2 is
232 required for its APC/C^{Cdh1}-dependent stability. IRS2's extended D-box (amino acids 972-
233 980 in human IRS2) is highly conserved in placental mammals despite overall divergence
234 in much of the C-terminus (**Figure 4A**), suggesting that this sequence likely has a
235 conserved function.
236 To test whether IRS2's full D-box is relevant for its Cdh1-dependent degradation,
237 we generated a mutant IRS2 construct bearing an R972A D-box mutation (DM), which
238 was expected to abrogate its function as a D-box [30]. To investigate the effect of
239 expressing the IRS2-DM construct in cells, we generated doxycycline-inducible, C-
240 terminally HA-tagged IRS2-WT and IRS2-DM RPE1 and C_2C_{12} cell lines. In an effort to
241 avoid saturating the system and overexpression artifacts, we sought to express tagged
242 IRS2 variants at low levels relative to the endogenous protein (**Figure S4A**).
243 Because we were able to detect the tagged proteins in the RPE1 cells without
244 adding doxycycline, we avoided using it in this cell line. As a caveat of this approach, we
245 observed a difference in the expression levels of the IRS2 WT and DM in RPE1 cells,
246 possibly due to differences in lentiviral titer upon cell line generation. Still, we
247 demonstrated that changes in transgene expression were quantifiable within the linear
248 range for both cell lines, making comparisons between controls (DMSO or control siRNA)

249 and APC/C inhibition (APC/C inhibitors or Cdh1 siRNA) quantifiable for each (**Figure**
250 **S4B**). Using these cell lines, we found that APC/C inhibition following G_1 arrest caused
251 accumulation of IRS2-WT but not IRS2-DM (**Figure 4B**). The degree of accumulation of
252 the WT protein depended on the dose of APC/C inhibitors used (**Figure S4C**).

253 In the C_2C_{12} cells stably expressing C-terminally HA-tagged IRS2 variants,
254 transgene expression was undetectable in differentiated myotubes in the absence of
255 doxycycline (data not shown), so we selected a low dose that maintained close-to-
256 endogenous expression levels in myoblasts (**Figure S4A**). Cells were differentiated for
257 three days in low-serum media. Following differentiation, myotubes were switched to new
258 media containing fresh doxycycline and either DMSO or APC/C inhibitors (the "0 hr" lane
259 in **Figure 4C**) and were collected 8 hours later. Due to the doxycycline refreshment,
260 myotubes exhibited a slight increase in transgene expression between 0 hours (the time
261 of drug addition) and 8 hours (the time of collection). We observed a strong increase in
262 levels of HA-tagged IRS2-WT in the presence of APC/C inhibitors compared to DMSO-
263 treated myotubes. In contrast, levels of HA-tagged IRS2-DM remained constant both in
264 the presence and absence of APC/C inhibitors (**Figure 4C**).

265 To further validate the Cdh1-dependence of IRS2's D-box motif, we asked whether
266 Cdh1 knockdown by siRNA could stabilize the IRS2-DM protein. Using asynchronous
267 RPE1 cells stably expressing C-terminally HA-tagged IRS2-WT and IRS2-DM, we found
268 that Cdh1 knockdown by siRNA caused an accumulation of IRS2-WT relative to control-
269 transfected cells but not IRS2-DM (**Figure 4D**). This result was repeated in HeLa cells
270 stably expressing N-terminally FLAG-HA-tagged IRS2-WT and IRS2-DM constructs
271 subject to the same conditions (**Figure 4E**).

272 IRS1 (the other primary adaptor protein for IGF1R and IR) shares 75% sequence
273 homology with IRS2's N-terminus and 35% homology with its C-terminus [31] but does
274 not share the D-box motif found in IRS2's C-terminus (**Figure 4F**). In keeping with our
275 hypothesis that Cdh1-mediated control of IRS2 is D-box dependent, IRS1 levels did not
276 increase in G_1-arrested RPE1 cells treated with APC/C inhibitors as measured by either
277 mass spectrometry (**Figure 4G**) or immunoblot (**Figure 4H**). Furthermore, while it did
278 display a change in electrophoretic mobility compatible with mitotic phosphorylation,
279 unlike IRS2, it did not decrease in abundance at mitotic exit in RPE1 cells (**Figure 4I**).

280 Taken together, the findings described above indicate that APC/C^{Cdh1} controls IRS2 levels
281 in manner that is dependent upon its C-terminal D-box motif.
282
283 *IRS2 is required for normal expression of many proteins involved in mitosis*
284 Many reported APC/C^{Cdh1} substrates (including several of those identified in our
285 initial proteomics screen) are required for normal cell cycle progression. Because
286 IR/IGF1R transduction promotes a variety of transcriptional programs [2], we
287 hypothesized that IRS2 might promote the expression of proteins involved in cell cycle
288 control. To investigate this, we generated two IRS2 knockout RPE1 cell lines using
289 CRISPR/Cas9 (**Figure 5A)**, henceforth referred to as ∆IRS2-A and ∆IRS2-B. Using these
290 cells, we again employed TMT-coupled quantitative proteomics. The proteomes of wild-
291 type, ∆IRS2-A, and ∆IRS2-B cell lines were analyzed in biological triplicate, and relative
292 abundances were ascertained based on TMT reporter ion signal-to-noise values.
293 Hierarchical clustering indicated that the proteomes of the two knockout cell lines
294 analyzed were more similar to each other than either knockout cell line was to wild-type
295 (**Figure S5A**), suggesting that deletion of IRS2 produced similar effects in both cell lines.
296 In order to exclude aberrancies that may have accrued during the CRISPR process or as
297 a result of clonal expansion, we focused the scope of our analysis to proteins that
298 changed significantly ($p < 0.05$) by more than 20% in both IRS2 knockout clones relative
299 to the WT cell line (**Figures 5B-5C**). We found 239 proteins that decreased by >20% in
300 both IRS2 knockout lines relative to the wild type line and 300 proteins that increased by
301 >20% (**Figures 5B-5C, S5B**).
302 We conducted gene enrichment analysis of the proteins that increased (**Figure**
303 **S5C-S5D**) or decreased (**Figure 5D**) by >20% in both knockout cell lines relative to wild
304 type cells. Of the 239 proteins that were depleted by >20% in both knockout cell lines, we
305 found a statistical over-representation of proteins participating in metabolic processes
306 characteristic of IR signal transduction. Notably, we also found an over-representation of
307 proteins involved in mitotic cell cycle regulation in this subset (**Figure 5D**). This suite of
308 proteins included regulators of mitotic entry and exit as well as several factors involved in
309 spindle assembly (**Figure 5E**). Importantly, IRS2 KO cells divide as the same rate as WT
310 cells (**Figure S6A-S6B**), indicating that this downregulation is not due to a bulk loss of

311 viability or cell cycle arrest. Consistent with the fact that strong depletion of most critical
312 cell cycle regulators renders cells inviable, most of the observed changes in cell cycle-
313 related genes were relatively modest (**Figure S6C**). Based on these data, we conclude
314 that IRS2 is important for promoting the expression of a suite of proteins involved in
315 orchestrating the mitotic cell cycle, and deletion of IRS2 stunts their expression in RPE1
316 cells.
317
318 *IRS2 expression promotes a functional spindle assembly checkpoint*
319 Because many of the factors that were depleted in IRS2 knockout cell lines are
320 involved in regulating the events of mitosis, we sought to investigate whether IRS2 KO
321 cell lines display phenotypic differences from wild-type cells under conditions of mitotic
322 stress—in this case, activation of the spindle assembly checkpoint (SAC). Using a high
323 content nuclear imaging assay to measure mitotic fraction [17], we asked whether IRS2
324 knockout cell lines display mitotic arrest differences compared to wild-type cells when
325 treated with spindle poisons. Wild-type cells treated with nocodazole (a microtubule
326 destabilizing agent) arrested in mitosis in a dose-dependent manner, whereas both IRS2
327 knockout cell lines displayed depressed mitotic arrest (**Figure 6A** and **Figure S7A**). This
328 was also true to a lesser extent in the presence of S-trityl-L-cysteine (STLC), an Eg5
329 inhibitor (**Figure 6A**). Importantly, this was not due to a reduction in the rate of mitotic
330 entry (**Figure S6B**).
331 We further evaluated this phenotype by live-cell imaging. Consistent with the
332 results from the fixed-cell assay, IRS2 knockout cell lines also had a significantly shorter
333 mitotic duration compared to wild-type cells ($p < 0.0001$ in both cases) when treated with
334 300 nM nocodazole (**Figure 6B** and **Figure S7B**). We next analyzed the effect of IRS2
335 knockout on APC/C activity in cells expressing mAG1-geminin (1-101), an APC/C^{Cdc20}
336 substrate that is stabilized by the spindle assembly checkpoint [32]. We found that wild-
337 type cells displayed an accumulation of mAG1 fluorescence early in mitotic arrest prior to
338 a gradual reduction due to leaky APC/C activity [33]. In contrast, both IRS2 knockout cell
339 lines display depressed mAG1 accumulation, followed by a more rapid loss of
340 fluorescence signal, consistent with higher APC/C^{Cdc20} activity due to a weakened
341 checkpoint (**Figure 6C**). This phenotype, along with the shorter mitotic duration and lower

342 mitotic fraction in the presence of spindle poisons, is consistent with cells bearing a
343 defective mitotic spindle assembly checkpoint. Based on these data, we conclude that
344 IRS2 expression promotes a functional spindle assembly checkpoint in RPE1 cells.
345
346 **Discussion**
347 Based on the results of an unbiased proteomic screen, we provide evidence that
348 IRS2, a critical mediator of IR/IGF1R signaling, is a direct APC/C^{Cdh1} substrate. We
349 demonstrate that IRS2 is stabilized by APC/C inhibition and Cdh1 knockdown in multiple
350 cell types and that this depends on IRS2's C-terminal D-box motif. In contrast, we find
351 that IRS1, a closely related IRS2 paralog that lacks a D-box, is not subject to regulation
352 by the APC/C. Taken together, these results show that APC/C activity directly controls
353 IRS2 levels in a D-box dependent manner.
354 We identified a high-mobility form of IRS2 that accumulates under APC/C
355 inhibition, likely corresponding to a difference in phosphorylation given that IRS2 has
356 ~150 annotated threonine, serine, and tyrosine phosphorylation sites [34]. This suggests
357 that IRS2's APC/C-dependent stability could be regulated by phosphorylation, possibly at
358 sites near or within the D-box, which is an intriguing topic for future study. Consistent with
359 this, IRS2 phosphorylation is known to impact its stability in other contexts, including
360 following prolonged exposure to insulin or following mTOR activation [2]. Furthermore,
361 there is a strong precedent for phospho-regulation of APC/C degrons modulating
362 substrate stability under specific conditions [35-37].
363 Many APC/C substrates are involved in cell cycle regulation, and previous studies
364 have suggested a relationship between IRS2 and cell cycle progression. IRS2 can
365 stimulate cell cycle entry via Cdk4 activation [38] and is important for sustaining
366 proliferation in 32D myeloid cells and pancreatic β cells [39, 40]. Based on these findings
367 and our identification of IRS2 as an APC/C substrate, we further investigated the role of
368 IRS2 in regulating cell division. Proteomic analyses of RPE1 cells lacking IRS2 reveal
369 lower expression of well-characterized cell cycle proteins compared to wild-type cells.
370 Because these proteins are involved in critical processes like cytokinesis, DNA
371 replication, cell cycle transitions, and spindle assembly, we investigated whether IRS2
372 knockout cell lines display cell cycle progression defects. We find that cells lacking IRS2

373 have an impaired ability to arrest following spindle assembly checkpoint activation in M-
374 phase, thereby implicating IRS2 in promoting a functional spindle assembly checkpoint.
375 Despite the well-established importance of sustained IRS2 levels in many tissue
376 types, little is known about what factors regulate its turnover. While several distinct
377 ubiquitin ligases control IRS1 stability (Fbxw8, Cbl-b, Fbxo40, SOCS1/3, MG53, and
378 others) [8-12], only SOCS1/3 have been implicated in the ubiquitin mediated proteolysis
379 of IRS2 [11] until now. Thus, our work establishes APC/C^{Cdh1} as the first known ubiquitin
380 ligase that targets IRS2 but not IRS1. Furthermore, our results suggest that APC/C^{Cdh1}-
381 mediated IRS2 degradation is relevant in broad biological contexts since we were able to
382 demonstrate this mechanism of regulation in multiple cell lines.
383 Over the past several years, a number of connections between growth factor
384 signaling and APC/C-mediated regulation have emerged. SKIL/SnoN, an APC/C
385 substrate involved in TGFβ signaling, implicates APC/C activity in modulating the
386 expression of TGFβ target genes [41]. Another APC/C substrate, CUEDC2, controls the
387 stability of the progesterone receptor [42]. Regarding IR/IGF1R signaling, connections to
388 APC/C-mediated regulation have been more opaque. Multiple reports have shown that
389 Cdh1 interacts with PTEN, a phosphatase that antagonizes signal transduction through
390 the IR pathway by dephosphorylating phosphoinositide-3,4,5-triphosphate (PIP_3) [43, 44].
391 Others have demonstrated that components of the mitotic checkpoint complex (which
392 inhibit APC/C^{Cdc20}) potentiates IR signaling via IR endocytosis [45, 46]. Despite these
393 links, there have been no reports of direct APC/C substrates that are involved in IR
394 signaling until now.
395 Based on the data presented here, we propose a model (**Figure 7**) in which IRS2's
396 APC/C-mediated degradation in G_1 serves to limit IRS2-dependent signaling during G_1.
397 Upon APC/C inactivation, IRS2 is able to accumulate and stimulate signaling required for
398 normal progression through the latter stages of the cell cycle, including the expression of
399 proteins required for mitotic spindle checkpoint function. This model is consistent with
400 previous studies that implicate IRS2 in promoting the expression of cell cycle-related
401 genes, including mitotic cyclins (A and B) in mouse granulosa cells [47]. Furthermore, IR
402 signal transduction promotes the expression of Plk1 (a mitotic kinase) and CENP-A (a

403 centromere protein) in β cells through a mechanism that appears to depend on IRS2
404 rather than IRS1 [40, 48].
405 Our findings suggest that APC/C^{Cdh1} modulates IRS2-dependent signaling but not
406 IRS1-dependent pathways. In IRS2-deficient mice with consequent type 2 diabetes, some
407 have attributed the reduced β cell mass to a failure of β cells to re-enter the cell cycle
408 following division [40]. Our findings that APC/C^{Cdh1} inhibition stabilizes IRS2 and that IRS2
409 promotes the expression of cell cycle regulatory proteins, coupled with data from others
410 showing that IRS2 can stimulate cell cycle entry [38], suggest that APC/C^{Cdh1} inhibition
411 may represent a possible approach for stimulating proliferation in quiescent β cells via
412 the stabilization of IRS2.
413
414 **Acknowledgements**
415 We thank the ICCB-Longwood Screening Facility at Harvard Medical School for
416 assistance with high content imaging assays and the Nikon Imaging Facility at Harvard
417 Medical School for assistance with time lapse and fluorescence microscopy. We thank
418 Kyle Copps, Pere Puigserver, and Christine Vogel for feedback on the manuscript. This
419 work was funded by NIH grant 1R35GM127032 to R.W.K and NIH grant GM67945 to
420 S.P.G.
421
422 **Author Contributions**
423 S.M. designed, performed, and analyzed all experiments aimed at identifying new APC/C
424 substrates in RPE1 cells. S.M. performed all experiments characterizing IRS2 as an
425 APC/C substrate. S.M. generated all recombinant cell lines used in this study and the
426 IRS2 CRISPR knockout cell lines. S.M. characterized mitotic arrest defects in IRS2
427 CRISPR knockout cell lines using time lapse microscopy and high-content imaging
428 assays. S.M. prepared all samples for mass spectrometry with assistance from Q.Y.
429
430 Q.Y. and S.P.G. performed mass spectrometry analysis of G_1 RPE1 cells treated with
431 APC/C inhibitors and IRS2 CRISPR knockout cell lines. Q.Y. and S.P.G. provided
432 reagents.
433

R.W.K. assisted with experimental design and data analysis.

S.M. and R.W.K. conceived of the project and wrote the manuscript with input from both other authors.

Declaration of Interests

The authors declare no competing financial interests.

Main Figure Legends

Figure 1: *High resolution chemical proteomics reveals proteins whose abundances are APC/C regulated.*

(A) Workflow for the chemical proteomics experiment described in this study. Asynchronous RPE1 cells were arrested in 1 μM palbociclib (a Cdk4/6 inhibitor) for 20 hours, at which point they were acutely treated with either DMSO or a combination of 6 μM proTAME + 50 μM apcin (referred to as "APC/C inhibitors" or "APC/Ci"). Cells were then collected at time 0 (the time of drug addition) or 8 hours after drug addition and were harvested for TMT-based proteomic identification and quantification. Samples were analyzed in biological triplicate within a 10-plex TMT label set, with the 10th channel used as a bridge.

(B) Asynchronous RPE1 cells were treated with either DMSO or 1 μM palbociclib for 20 hours. Cells were harvested, and lysates were analyzed by immunoblot for the indicated proteins.

(C) Previously reported APC/C substrates that were identified in this study are plotted with their observed fold change in the APC/C inhibitor treated sample (APC/Ci) relative to the DMSO treated sample. Error bars represent the standard deviation (SD) between the three biological replicates measured by MS. Asterisks indicate an abundance increase over control that is statistically significant (* : $p < 0.05$; ** : $p < 0.01$; *** : $p < 0.001$; **** : $p < 0.0001$)

(D) Previously reported APC/C substrates that were identified as increasing by mass spectrometry in G_1 RPE1 cells treated with APC/C inhibitors were validated by immunoblot for selected proteins.

465 (E) Volcano plot highlighting all published APC/C substrates identified in this study (blue)
466 as well as proteins that (1) contain a high probability D- and/or KEN-box (D-box =
467 green, KEN-box = pink, D- and KEN-boxes = purple), (2) increase ≥1.15-fold under
468 APC inhibition, (3) were identified by >1 peptide, and (4) have a *p*-value < 0.05.
469
470 ***Figure 2***: *IRS2 levels are controlled by Cdh1 in a proteasome-dependent manner*
471 (A) Cells were treated identically to what is described in **Figure 1A**, and IRS2 abundance
472 was measured by immunoblot.
473 (B) C_2C_{12} myoblasts were induced to differentiate through serum withdrawal and
474 supplementation with insulin, transferrin, and selenium (ITS). After three days of
475 differentiation, myotubes were acutely treated with either DMSO or APC/C inhibitors
476 (of 6 μM proTAME + 50 μM apcin). After eight hours of drug treatment, myotubes were
477 collected and IRS2 levels from all samples were analyzed by immunoblotting.
478 (C)– (D) Asynchronous HeLa (*C*) and RPE1 (*D*) cells were transfected with either a
479 control or Cdh1-directed siRNA for 24 hours. Cells were allowed to grow for an
480 additional 24 hours prior to collection and analysis of the indicated protein levels in
481 lysate by immunoblot.
482 (E) HeLa cells were mock transfected or transfected with increasing amounts of a
483 plasmid encoding myc-tagged human Cdh1 for 24 hours. Cells were allowed to grow
484 for an additional 24 hours prior to collection and analysis of the indicated protein
485 levels by immunoblot.
486 (F) RPE1 cells were arrested in G_1 with 1 μM palbociclib for 20 hours. Following G_1
487 arrest, cells were treated with DMSO, APC/C inhibitors (6 μM proTAME + 50 μM
488 apcin), MG132 (10 μM), or a combination of APC/C inhibitors and MG132 for an
489 additional 8 hours. Cells were harvested, and lysates were analyzed by immunoblot
490 for IRS2 abundance.
491 (G) 6x-His-tagged ubiquitin conjugates were isolated from HeLa cell lysates using Ni-
492 NTA agarose resin. Lysates were derived from cells expressing 6x-His-ubiquitin and
493 HA-tagged IRS2 that were treated with MG132 alone or in combination with APC/C
494 inhibitors. Resin eluate and inputs were probed by immunoblot using an HA antibody,
495 and Ponceau staining was used as a loading control.

496 ***Figure 3***: *IRS2 levels and phosphorylation fluctuate in a cell-cycle dependent manner*

497 (A) HeLa cells were synchronized by double thymidine block and released into S-phase
498 in the presence of nocodazole. Lysates were harvested and analyzed by
499 immunoblotting for IRS2 and cell cycle markers.

500 (B) HeLa cells were synchronized by single thymidine-nocodazole block and released into
501 prometaphase. Mitotic cells were collected by mitotic shake-off and re-plated. Time
502 points were taken every two hours as cells exited M-phase. Lysates were harvested
503 and analyzed by immunoblotting for IRS2 and cell cycle markers.

504 (C) RPE1 cells were synchronized in G_2 by treatment with the Cdk1 inhibitor RO3306.
505 After 18 hours, cells were switched to fresh media and were allowed to enter mitosis
506 (~35 minutes following drug removal). At mitotic entry, cells were collected by mitotic
507 shake-off and were re-plated (0 hr). Time points were taken as cells exited M-phase
508 and entered G_1. Lysates were harvested and analyzed by immunoblotting for IRS2
509 and cell cycle markers.

510

511 ***Figure 4***: *Cdh1's ability to control IRS2 levels depends on a C-terminal D-box motif*

512 (A) (*top*) Schematic depicting IRS2's protein domain structure. PH = pleckstrin homology
513 domain, PTB = phosphotyrosine binding domain, KRLB = kinase regulatory-loop
514 binding region. IRS2's C-terminal full D-box motif is highlighted in red. (*bottom*)
515 Comparison of IRS2's D-box conservation among placental mammals.

516 (B) RPE1 cells stably expressing lentivirus-derived, doxycycline-inducible, C-terminally
517 HA-tagged IRS2 constructs were arrested in G_1 with 1 μM palbociclib for 20 hours in
518 the absence of doxycycline. Following arrest, samples were either collected or DMSO
519 or APC/C inhibitors (6 μM proTAME + 50 μM apcin) were added for an additional 8
520 hours. Quantification of immunoblots shown at right: HA levels were normalized to a
521 loading control and are plotted relative to DMSO levels. Error bars = mean ± SEM. * :
522 $p = 0.0187$; ns : $p = 0.816$

523 (C) C_2C_{12} myoblasts stably expressing lentivirus-derived, doxycycline-inducible, C-
524 terminally HA-tagged IRS2 constructs were grown to confluence and switched to low
525 serum media supplemented with ITS (differentiation media) and doxycycline. Cells
526 were allowed to differentiate into myotubes for three days (with media refreshment

527 every 24 hours), at which point (0 hr) either DMSO or APC/C inhibitors (6 μM proTAME
528 + 50 μM apcin) for an additional 8 hours in the presence of doxycycline. Quantification
529 of immunoblots shown at right: HA levels were normalized to a loading control and are
530 plotted relative to DMSO levels. Error bars = mean ± SEM. * : p = 0.0118; ns : p =
531 0.910.
532 (D) Asynchronous RPE1 cells stably expressing lentivirus-derived, doxycycline-inducible
533 C-terminally HA-tagged IRS2 constructs were transfected with a non-targeting
534 (control) siRNA or an siRNA directed against Cdh1 for 24 hours in the absence of
535 doxycycline. Quantification of immunoblots shown at right: HA levels were normalized
536 to a loading control and are plotted relative to DMSO levels. Error bars = mean ± SEM.
537 * : p = 0.0132; ns : p = 0.963.
538 (E) Asynchronous HeLa cells stably expressing lentivirus-derived, N-terminally FLAG-HA
539 tagged IRS2 constructs were transfected with a non-targeting (control) siRNA or an
540 siRNA directed against Cdh1 for 24 hours. Quantification of immunoblots shown at
541 right: HA levels were normalized to a loading control and are plotted relative to DMSO
542 levels. Error bars = mean ± SEM. * : p = 0.0131; ns : p = 0.803.
543 (F) Comparison of the Hs IRS2 D-box sequence with the corresponding region from Hs
544 IRS1.
545 (G) MS-quantified IRS1 and IRS2 abundance in G_1 APC inhibitor proteomics (**Figure 1**).
546 IRS1 abundance was quantified based on 5 peptides (4 unique) in 3 biological
547 replicates; IRS2 was quantified based on 3 peptides (all unique) in 3 biological
548 replicates.
549 (H) RPE1 cells were subject to the same conditions described in **Figure 1A**, and cell
550 lysates were analyzed by immunoblotting for IRS1 abundance
551 (I) RPE1 cells were treated as in **Figure 3C**. Cell lysates were analyzed by
552 immunoblotting for IRS1 abundance.
553
554 ***Figure 5***: *IRS2 knockout cell lines are defective in mitotic cell cycle-related protein*
555 *expression*.
556 (A) WT, ΔIRS2-A, and ΔIRS2-B cell line lysates were analyzed for IRS2 expression by
557 immunoblotting.

558 (B-C) Volcano plots comparing proteomes of ΔIRS2 cell lines with WT cell line. Proteins
559 that significantly decrease > 20% (*p*-value < 0.05) in both cell lines compared to wild-
560 type are shown in purple; proteins that significantly increase > 20% (*p*-value < 0.05)
561 in both cell lines compared to WT are shown in green.
562 (D) Gene ontology (GO) term enrichment of proteins that decrease in both ΔIRS2 cell lines
563 relative to WT cells.
564 (E) Heat map depicting cell cycle-related protein abundance changes between ΔIRS2 cell
565 lines and WT cells.
566
567 ***Figure 6***: *IRS2 expression promotes a functional spindle assembly checkpoint.*
568 (A) Analysis of fraction of cells in mitosis for RPE1 wild type (WT) and IRS2 KO cell lines
569 treated with the indicated doses of nocodazole and S-trityl L-cysteine (STLC) for 18
570 hours. Mitotic fraction measurements were made using a high content fixed cell
571 imaging assay based on DAPI intensity of stained nuclei. Error bars = mean ± SD.
572 (B) Asynchronous RPE1 wild type (WT) or IRS2 KO cell lines were treated with 300 nM
573 nocodazole and imaged every five minutes by widefield time lapse microscopy for 36
574 hours. Each point represents an individual cell's mitotic duration, measured as the
575 time from nuclear envelope breakdown (NEB) to division, slippage, or cell death. Error
576 bars = mean± SD. *p*-values were calculated by one-way ANOVA. **** = $p < 0.0001$.
577 ns = not statistically significant.
578 (C) Asynchronous RPE1 wild type (WT) or IRS2 KO cell lines expressing mAG1-
579 geminin(1-110) were treated as in (C). mAG1 fluorescence intensity was measured
580 from nuclear envelope breakdown (NEB) until division, slippage, or cell death (n = 10
581 for all three cell lines). Error bars = mean ± SEM. Fluorescence intensity was
582 background subtracted and normalized to intensity at NEB.
583
584 ***Figure 7***: Model for IRS2's role in cell cycle control. IRS2 is targeted for proteasomal
585 degradation by APC/C^{Cdh1} during G_1. When APC/C is inactivate, IRS2 protein
586 accumulates, potentially allowing it to stimulate the expression of cell cycle-related
587 proteins either through IR-mediated action [48] or through another receptor tyrosine
588 kinase. Some of the proteins that are expressed through this pathway may be required

589 for a robust spindle assembly checkpoint, which directly inhibits APC/C^{Cdc20} during M-
590 phase.
591
592 **Tables**
593 ***Table 1*:** 26 proteins containing high-probability D- and KEN-boxes as identified from G_1
594 APC/C inhibitor proteomics.
595

Gene Symbol	Fold Change (APC/Ci : DMSO)	Similarity Score	Disorder Score	Reference (if applicable)
D-box containing proteins				
IRS2	1.3	0.87	0.68	
PBXIP1	1.2	0.83	0.42	[49]
DCBLD1	1.2	0.86	0.56	
ULK1	1.2	0.85	0.58	
NAA38	1.2	0.82	0.44	
LRP10	1.2	0.82	0.49	
CEP120	1.2	0.84	0.42	
DIAPH3*	1.2	0.84	0.56	[50]
ANKRD11	1.2	0.86	0.53	
KEN-box containing proteins				
TK1	3.6	0.97	0.53	[26]
TACC3	1.9	0.94 / 0.90	0.54 / 0.49	[51]
TOP2A	1.8	0.86	0.44	[27]
MKI67	1.5	0.89 / 0.86	0.45 / 0.48	
CUEDC2	1.4	0.99	0.71	[52]
GPBP1	1.3	0.81	0.61	
UHRF2	1.2	0.88	0.61	
KIF23	1.2	0.87	0.45	[53]
PNPLA8	1.2	0.92	0.61	
KDM2A	1.2	0.94	0.66	
PRPF38B	1.2	0.92	0.44	
DLGAP5	1.2	0.89	0.6	[54]
D- and KEN-box containing proteins				
CKAP2	3.2	D:0.95 K: 0.81	D: 0.59 K: 0.48	[55]
KIF11	2.4	D: 0.95 K: 0.81	D: 0.62 K: 0.49	[56]

GMNN**	2.2	D: 0.97 K: 0.84	D: 0.57 K: 0.52	[57]
KDM3A	1.2	D: 0.80 K: 0.81	D: 0.61 K: 0.66	
BUB1B	1.2	D: 0.92 / 0.85 K: 0.83 / 0.86	D: 0.47/0.64 K: 0.47/0.49	[58]

596

597 Features of the putative degron(s) found in each protein are annotated, including the
598 SLiMSearch similarity score to other validated degrons, the similarity of the surrounding
599 consensus sequence to other validated degrons, the disorder score for the region of the
600 protein in which the degron is located, and the citation of the publication that reports the
601 protein as an APC/C substrate, where applicable. *While DIAPH3/mDia2 has been shown
602 to be ubiquitinated in a cell cycle dependent manner and was suggested as an APC/C
603 substrate, there is no direct cell-based or biochemical evidence for this. **We cannot
604 delineate whether the geminin peptides identified here derive from the FUCCI reporter or
605 the endogenous protein. Proteins that have not been previously reported as APC/C
606 substrates are shown in bold.

607

608 **Experimental Procedures**

609 ***Cell Culture and Synchronization***

610 All cell lines used in this work (HeLa, C_2C_{12}, hTERT-RPE1-FUCCI, HEK293T) were
611 cultured in a humidified incubator at 37ºC in the presence of 5% CO_2. HeLa, hTERT-
612 RPE1 and C_2C_{12} cells were obtained from American Type Culture Collection (ATCC), and
613 hTERT-RPE1 cells were modified with FUCCI constructs [20] with the permission of the
614 RIKEN Institute. HeLa cells were grown in DMEM with 10% FBS. Proliferating C_2C_{12}
615 myoblasts were grown in DMEM with 15% FBS, whereas differentiated myotubes were
616 cultured in differentiation media, consisting of DMEM with 2% horse serum and 1x insulin,
617 transferrin, selenium (ITS) Premix Universal Culture Supplement (Corning, 354350).
618 hTERT-RPE1-FUCCI cells were grown in DMEM/F12 with 10% FBS supplemented with
619 0.01 mg/ml hygromycin B (Corning, 30-240-CR). HEK293T cells used for lentivirus
620 generation were a gift from Wade Harper and were cultured in DMEM with 10% FBS. All
621 cell lines tested were negative for mycoplasma contamination (Lonza LT07-218).

622

623 HeLa cells were synchronized by double thymidine block by treating with 2 mM thymidine
624 for 18 hours, releasing for 8 hours, and re-treating with 2 mM thymidine for 19 hours.
625 HeLa cells synchronized by thymidine-nocodazole block were treated with 2 mM
626 thymidine for 20 hours, released for 8 hours, then treated with 300-330 nM nocodazole
627 for 15 hours. Mitotic cells were collected by shake-off and re-plated in drug-free media for
628 cell cycle time course experiments.

629

630 RPE1 cells were synchronized by RO3306 treatment by treating with 7.5 μM RO3306 for
631 18 hours before releasing into fresh media for 30-40 minutes, after which cells were
632 collected by mitotic shake-off and re-plated for cell cycle time course experiments. For G_1
633 arrest experiments, RPE1 cells were treated with 1 μM palbociclib for 20 hours.

634

635 To differentiate C_2C_{12} myoblasts into myotubes, cells were grown to confluence and
636 washed 2x in DMEM with 2% horse serum before switching to differentiation media. Cells
637 were incubated for 72 hours, with media changes every 24-36 hours. Differentiation into
638 myotubes was monitored visually as well as by immunoblotting for MyoD, a myogenic
639 marker.

640

641 ***Immunoblotting***

642 Cell extracts were prepared in lysis buffer (10 mM Tris HCl pH 7.4, 100 mM NaCl, 1 mM
643 EDTA, 1 mM EGTA, 1 mM NaF, 1 mM PMSF, 20 mM $Na_4P_2O_7$, 2 mM NA_3VO_4, 1% Triton
644 X-100, 10% glycerol, 0.1% SDS, and 0.5% deoxycholate) supplemented with Pierce
645 protease inhibitor tablets (Thermo Fisher Scientific, A32963) and Pierce phosphatase
646 inhibitor tablets (Thermo Fisher Scientific, A32957). Pellets were incubated in lysis buffer
647 on ice for 30 minutes with vortexing and were centrifuged at 13,000rpm for 10 minutes to
648 clear the lysate. Protein concentrations were determined using a bicinchoninic acid (BCA)
649 assay (Thermo Fisher Scientific, 23225). Supernatants were re-suspended in NuPAGE
650 LDS sample buffer (Thermo Fisher Scientific, NP0008) supplemented with 100 mM
651 dithiothreitol (DTT) and boiled at 100ºC for 5 minutes. Equal masses of lysates were
652 separated by SDS-PAGE using either 4-12% Bis Tris gels or 3-8% Tris acetate gels

653 (Thermo Fisher Scientific). All IRS2 immunoblots were separated on 3-8% Tris acetate
654 gels with the exception of those shown in **Figures 5A** and **S4B**, which were separated on
655 4-12% Bis Tris gels. Proteins were transferred to polyvinylidene difluoride (PVDF)
656 membranes (Thermo Fisher Scientific, 88518).
657
658 Membranes were blocked in 5% non-fat dry milk in Tris-buffered saline with 0.1% Tween
659 (TBS-T) before incubating with primary antibodies overnight at 4ºC with agitation.
660 Membranes were probed with secondary antibodies dissolved in 5% milk in TBS-T for 1-
661 2 hours at room temperature before developing with an Amersham 600RGB imaging
662 system. Quantification of immunoblots was done using ImageJ [59].
663
664 ***Antibodies***
665 The following commercially available primary antibodies were used for immunoblotting:
666 anti-IRS2 (Cell Signaling Technologies, 4502) 1:750; anti-Cdh1/Fzr1 (Sigma Aldrich,
667 CC43) 1:500; anti-anillin [60] 1:1000; anti-Aurora B (Bethyl, A300-431) 1:1000; anti-Eg5
668 (Cell Signaling Technologies, 4203) 1:1000; anti-Top2A (Cell Signaling Technologies,
669 12286) 1:1000; anti-TK1 (Cell Signaling Technologies, 8960) 1:1000; anti-Mps1 (Abcam,
670 ab11108), 1:1000); anti-APC3 (BD Transduction Laboratories, 610455) 1:500; anti-cyclin
671 B1 (Santa Cruz Biotechnology, sc-752) 1:500; anti-Cdc20 (Santa Cruz Biotechnology, sc-
672 8358) 1:500; anti-c-Myc (9E10, Santa Cruz Biotechnology, sc-40) 1:1000; anti-HA-
673 peroxidase (Sigma Aldrich), 1:1500; anti-cyclin A2 (Santa Cruz Biotechnology, sc-596)
674 1:500; anti-IRS1 (Cell Signaling Technologies, 2382) 1:750; anti-MyoD1 (Cell Signaling
675 Technologies, 13812) 1:750; anti-GAPDH (Abcam, ab8245) 1:2000; anti-α tubulin
676 (Abcam, ab7291 and Santa Cruz Biotechnology, sc-8035) 1:1000 for both; anti-vinculin
677 (Santa Cruz Biotechnology, sc-73614) 1:2000. Secondary antibodies used: anti-rabbit
678 IgG-HRP (GE Healthcare, NA934) and anti-mouse IgG- HRP (GE Healthcare, NA931V),
679 both at 1:3000 dilutions.
680
681 ***Compounds***
682 The following chemicals were used: palbociclib (LC Laboratories, P-7722), proTAME
683 (Boston Biochem, I-440), MG132 (474790, Calbiochem), S-trityl L-cysteine (STLC, Alfa

684 Aesar, L14384), thymidine (Sigma Aldrich, T9250), nocodazole (Sigma Aldrich, 31430-
685 18-9), RO3306 (AdipoGen Life Sciences, AGCR13515M), doxycycline hyclate (Sigma
686 Aldrich, D9891). Apcin was custom synthesized by Sundia MediTech Company (Lot
687 #A0218-10069-031) using methods described previously [17]. All compounds were
688 dissolved in dimethyl sulfoxide (DMSO), with the exception of thymidine and doxycycline,
689 which were dissolved in Dulbecco's phosphate buffered saline (DPBS, Corning, 21-030-
690 CV). Dissolved compounds were stored at -20°C prior to use.
691
692 ***CRISPR/Cas9 mediated gene editing***
693 A TrueGuide crRNA directed against exon 1 of Hs IRS2's coding region (target DNA
694 sequence: 5'- TCG AGA GCG ATC ACC CGT TT -3', Assay ID number:
695 CRISPR850215_CR, Thermo Fisher Scientific) was annealed to the TrueGuide tracrRNA
696 (Thermo Fisher Scientific, A35507) according to manufacturer protocol. hTERT RPE1-
697 FUCCI cells were co-transfected with TrueCut Cas9 protein v2 (Thermo Fisher Scientific,
698 A36496) and the annealed tracrRNA:crRNA complex using the Lipofectamine
699 CRISPRMAX Cas9 Transfection reagent (Thermo Fisher Scientific, CMAX00003)
700 according to manufacturer protocol. Transfected cells were incubated for two days before
701 switching to fresh media and expanding. Single cell clones were isolated using the limiting
702 dilution method in a 96-well format, and clonal cell lines were expanded before screening
703 for knockouts by immunoblotting.
704
705 ***Site directed mutagenesis***
706 R777-E111 Hs.IRS2 and R777-E111 Hs.IRS2-nostop were gifts from Dominic Espositio
707 (Addgene plasmid #70395 and #70396, respectively). Both of these plasmids encode
708 codon optimized sequences for IRS2, with and without a stop codon respectively. R972A
709 mutations were introduced into the aforementioned IRS2 clones using the Q5 Site-
710 Directed Mutagenesis Kit (New England BioLabs) with the primers 5' - AGA TTA TAT
711 GAA TAA GTC CAC TGT CAG ATT ATA TG - 3' and 5' - GAC AGT GGA CTT GCC TGG
712 CGA GAG TCT GAA CT - 3' according to the manufacturer's protocol. For N-terminally
713 FLAG-HA-tagged constructs, the insert from R77-E111 Hs.IRS2 (WT or) was cloned into
714 the pHAGE-FLAG-HA-NTAP vector (a gift from Wade Harper) using the Gateway LR

715 Clonase II system (Invitrogen). For doxycycline-inducible, C-terminally HA-tagged
716 constructs, the insert from R77-E111 Hs.IRS2-nostop (WT or DM) was cloned into
717 pINDUCER20 (a gift from Stephen Elledge, Addgene plasmid #44012) using the Gateway
718 LR Clonase II system (Invitrogen). The DM mutation was verified both before and after
719 Gateway cloning by Sanger sequencing.
720
721 ***Lentivirus construction***
722 To construct lentiviruses, HEK293T cells were co-transfected with pPAX2, pMD2, and
723 either pINDUCER-20-IRS2 or pHAGE-FLAG-HA-NTAP-IRS2 in a 4:2:1 DNA ratio using
724 Lipofectamine 3000 (Invitrogen, L3000001) according to manufacturer's instructions.
725 pPAX2 and pMD2 were gifts from Wade Harper. 24 hours after transfection, HEK293T
726 cells were switched to fresh media (DMEM + 10% FBS). 48 hours after transfection
727 lentiviruses were harvested by clearing debris by centrifugation at 960*xg* for 5 minutes
728 and filtering through 0.45 µm SFCA filters. Lentiviruses were either used immediately or
729 flash frozen in liquid nitrogen and stored at -80ºC for later use.
730
731 ***Stable cell line construction***
732 To generate stable cell lines, plated HeLa, RPE1, or C_2C_{12} cells were incubated with
733 lentiviruses and 2 µg/ml protamine sulfate. 24 hours after viral infection, cells were
734 switched to fresh media. 48 hours after viral infection, antibiotics were introduced. For
735 lentiviruses derived from pINDUCER20, geneticin (Invitrogen, 10131027) was used at a
736 concentration of 750 µg/ml for both RPE1 and C_2C_{12} for 6-7 days. For lentiviruses derived
737 from pHAGE-FLAG-HA-NTAP, puromycin (Sigma Aldrich, P8833) was used at a
738 concentration of 0.5 µg/ml for 3 days. Antibiotic-selected populations of cells were
739 expanded and used for further experiments without clonal selection.
740
741 ***Small interfering RNAs (siRNAs)***
742 Cells were transfected using RNAiMax (Invitrogen, 13778100) according to
743 manufacturer's instructions with the following siRNAs: siGENOME Non-Targeting Control
744 siRNA #5 (D-001210-05, Dharmacon); ON-TARGETplus Human FZR1 siRNA (J-015377-
745 08, Dharmacon), 25 nM; SMARTpool ON-TARGETplus Mouse Fzr1 siRNA (L-065289-

746 01-0005), 25 nM. Cells were treated with siRNAs for 24 hours for all experiments. For
747 experiments involving subsequent compound treatment, cells were switched to fresh
748 media prior to the addition of compounds.
749
750 ***Plasmid transfection***
751 C_2C_{12} myoblasts were transfected with a plasmid containing the N-terminal 88 amino
752 acids of human cyclin B1 fused to EGFP using Lipofectamine 3000 (Invitrogen,
753 L3000001) with the P3000 reagent according to manufacturer's instructions. Growth
754 media was refreshed to remove transfection reagents 24 hours post-transfection, and
755 cells were switched to differentiation media for an additional 3 days.
756
757 For ubiquitination studies, HeLa cells were transfected with equal amounts of pCI-6xHis-
758 hUb and/or pHAGE-NTAP-IRS2 using Lipofectamine 3000 with the P3000 reagent
759 according to manufacturer's instructions. For myc-Cdh1 overexpression studies, HeLa
760 cells were transfected with 0, 0.5, 1, and 2 µg of pCS2+ myc-hCdh1 using Lipofectamine
761 3000 with the P3000 reagent according to manufacturer's instructions.
762
763 ***In vivo ubiquitination assay***
764 HeLa cells expressing pCI-6xHis-hUb and pHAGE-NTAP-IRS2 were treated with 10 µM
765 MG132 either alone or in the presence of APC/C inhibitors (6 µM proTAME + 50 µM
766 apcin) for 8 hours. Following drug treatment, cells were collected, washed in Dulbecco's
767 Phosphate Buffered Saline with calcium and magnesium (Corning, 21-030-CM), and flash
768 frozen in liquid nitrogen. Cell pellets were lysed in denaturing lysis buffer (8M urea; 100
769 mM Na_2HPO_4; 0.05% Tween-20; 10 mM imidazole HCl, pH 8.0; 100 mM Tris HCl, pH 8.0;
770 1x protease inhibitor cocktail) by periodic vortexing on ice. Lysates were cleared at 13,000
771 rpm for 10 minutes. Protein concentrations were measured by BCA assay. Equal amounts
772 of protein were incubated with Ni-NTA agarose resin (Qiagen, 30210) for four hours,
773 rotating at 4°C. Resins were washed three times in denaturing wash buffer (8M urea; 100
774 mM Na_2HPO_4; 0.05% Tween-20; 20 mM imidazole HCl, pH 8.0; 100 mM Tris HCl, pH 8.0)
775 followed by three washes in native wash buffer (100 mM Na_2HPO_4; 0.05% Tween-20; 20
776 mM imidazole HCl, pH 8.0; 100 mM Tris HCl, pH 8.0). His-ubiquitin conjugates were

777 eluted by boiling resin in 2x LDS sample buffer (Thermo Fisher Scientific, NP0008)
778 supplemented with 200 mM DTT and 200 mM imidazole HCl, pH 8.0 for 10 minutes. Input
779 samples were resolved on 4-12% Bis-Tris gels (Thermo Fisher Scientific), and Ni-NTA
780 elution samples were resolved on 3-8% Tris acetate gels (Thermo Fisher Scientific).
781 Ponceau staining was used as a loading control.
782
783 ***Time lapse and fluorescence microscopy***
784 Cells were plated in a 24-well coverslip-bottom plate (Greiner BioOne, 662892). After 24
785 hours, cells were treated with the indicated compounds and were imaged immediately
786 afterwards. Plates were inserted into a covered cage microscope incubator (OkoLab) with
787 temperature and humidity control at 37ºC and 5% CO_2 and mounted on a motorized
788 microscope stage (Prior ProScan III). All images were collected on a Nikon Ti motorized
789 inverted microscope equipped with a 20x/0.75 NA Plan Apo objective lens and the Perfect
790 Focus system. mCherry fluorescence was excited with a Lumencor Spectra-X using a
791 555/25 excitation filter and a 605/52 emission filter (Chroma). mAG1 fluorescence was
792 excited using a 490/20 excitation filter and a 525/36 emission filter (Chroma). Both
793 configurations used a Sedat Quad dichroic (Chroma). Images were acquired with a
794 Hamamatsu Orca-R2 or Hamamatsu Flash 4.0 V2 controlled with Nikon Elements image
795 acquisition software. Three fields of view were collected per condition, and phase contrast
796 and/or fluorescence images were captured at 5- to 8-minute intervals (depending upon
797 the experiment) for 24-48 hours.
798
799 Videos were analyzed using ImageJ. Mitotic duration was defined as the time from
800 nuclear envelope breakdown (NEB) until division, death (cytoplasmic blebbing), or mitotic
801 slippage. mAG1 and mCherry intensities were quantified manually by measuring the
802 maximum intensity of signal for each cell in a given frame across multiple time points. For
803 experiments analyzing fluorescence intensity during G_1 arrest, measurements were made
804 for all cells in a frame for each time point.
805
806 ***Experimental design and statistical rationale***

807 For G_1 proteomics experiments, cells were treated with 1 μM palbociclib for 20 hours at
808 which point cells were either collection (t_0) or treated with DMSO (control) or APC/C
809 inhibitors (6 μM proTAME + 50 μM apcin) for an additional 8 hours prior to collection
810 (n=3). For IRS2 knockout proteomic analysis, the proteomes of one control cell line (which
811 had been subject to the CRISPR process but expressed wild-type levels of IRS2) and two
812 distinct clonal IRS2 knockout lines were measured (n=3). For both G_1 APC/C inhibitor
813 proteomics and IRS2 knockout cell line analysis, samples were analyzed in biological
814 triplicate (e.g. from separate starter cultures) to increase statistical power. Technical
815 replicates were not measured for either experiment. No samples were excluded from
816 either analysis. Peptide spectral matches were filtered with a linear discriminant analysis
817 (LDA) method to a 1% FDR [61] and a protein-level FDR of 1% was also implemented
818 [62]. For both datasets, comparisons were calculated using a two-tailed, unpaired
819 Student's t-test. For the G_1 proteomics experiment, we considered significantly changing
820 proteins as those with a p-value<0.05 that increased ≥1.15-fold (based on the fold-
821 changes observed for previously reported APC/C substrates within our dataset). For the
822 IRS2 knockout cell line analysis, we considered significantly changing proteins as those
823 with a p-value<0.05 and a <20% change in abundance. For experiments regarding the
824 stability of IRS2-WT and IRS2-DM, p-values were calculated by two-way ANOVA. For
825 fluorescence microscopy experiments that quantify mAG1 intensity in response to drug
826 treatment over time, p-values were calculated by two-way ANOVA. For microscopy
827 experiments that quantify mitotic duration following nocodazole treatment, p-values were
828 calculated by one-way ANOVA. For time lapse microscopy data, p-values were calculated
829 by one-way ANOVA. Gene enrichment was calculated using the AmiGO 2 search tool
830 [63]. Error bars represent standard deviation (SD) or standard error of the mean (SEM)
831 where indicated.
832
833 ***TMT mass spectrometry sample preparation***
834 Cells were cultured as described in biological triplicate. Cells pellets were re-suspended
835 in urea lysis buffer: 8M urea, 200 mM EPPS pH 8.0, Pierce protease inhibitor tablets
836 (Thermo Fisher Scientific, A32963), and Pierce phosphatase inhibitor tablets (Thermo
837 Fisher Scientific, A32957). Lysates were passed through a 21-gauge needle 20 times,

838 and protein concentrations were measured by BCA assay (Thermo Fisher Scientific). 100
839 µg of protein were reduced with 5 mM tris-2-carboxyethyl-phosphine (TCEP) at room
840 temperature for 15 minutes, alkylated with 10 mM iodoacetamide at room temperature for
841 30 minutes in the dark, and were further reduced with 15 mM DTT for 15 minutes at room
842 temperature. Proteins were precipitated using a methanol/chloroform extraction. Pelleted
843 proteins were resuspended in 100 µL 200 mM EPPS, pH 8.0. LysC (Wako, 125-05061)
844 was added at a 1:50 enzyme:protein ratio, and samples were incubated overnight at room
845 temperature with agitation. Following overnight incubation, trypsin (Promega, V5111) was
846 added at a 1:100 enzyme:protein ratio, and samples were incubated for an additional 6
847 hours at 37ºC. Tryptic digestion was halted by the addition of acetonitrile (ACN). Tandem
848 mass tag (TMT) isobaric reagents (Thermo Fisher Scientific, 90406) were dissolved in
849 anhydrous ACN to a final concentration of 20 mg/mL, of which a unique TMT label was
850 added at a 2:1 label:peptide ratio. Peptides were incubated at room temperature for one
851 hour with vortexing after 30 minutes. TMT labeling reactions were quenched by the
852 addition of 10 µL of 5% hydroxylamine. Equal amounts of each sample were combined
853 at a 1:1 ratio across all channels and lyophilized by vacuum centrifugation. Samples were
854 re-suspended in 1% formic acid (FA)/99% water and were desalted using a 50 mg 1cc
855 SepPak C18 cartridge (Waters, WAT054955) under vacuum. Peptides were eluted with
856 70% ACN/1% FA and lyophilized to dryness by vacuum centrifugation. The combined
857 peptides were fractionated with basic pH reversed-phase (BPRP) HPLC, collected in a
858 96-well format and consolidated to a final of 24 fractions, out of which only alternating
859 fractions (a total of 12) were analyzed [64]. Each fraction was desalted via StageTip,
860 lyophilized to dryness by vacuum centrifugation, and reconstituted in 5% ACN/5% FA for
861 LC-MS/MS processing.
862
863 ***TMT mass spectrometry analysis***
864 Data for the G_1 APC/C inhibition experiment were collected on an Orbitrap Fusion mass
865 spectrometer coupled to a Proxeon EASY-nLC 1000 liquid chromatography (LC) pump
866 (Thermo Fisher Scientific), whereas data for IRS2 knockout cell line analysis were
867 collected on an Orbitrap Fusion Lumos mass spectrometer coupled to a Proxeon EASY-
868 nLC 1200 liquid chromatography (LC) pump. The 100 µm capillary column was packed

869 with 30 cm of Accucore 150 resin (2.6 µm, 150Å; Thermo Fisher Scientific). Mobile
870 phases were 5% ACN, 0.125% FA (Buffer A) and 95% ACN, 0.125% FA (Buffer B).
871 Peptides from G_1 APC/C inhibition experiment were separated using a 2.5 h gradient from
872 4% to 26% Buffer B and analyzed with a SPS-MS3 method [65]. Peptides from IRS2
873 knockout cell line analysis were separated using a 2 h gradient from 4% to 30% Buffer B
874 and analyzed with a real-time search strategy [66, 67]. The mass spectrometry
875 proteomics data have been deposited to the ProteomeXchange Consortium via the
876 PRIDE [68] partner repository with the dataset identifier PXD018329 and
877 10.6019/PXD018329.
878
879 Raw data were converted to mzXML format using a modified version of RawFileReader
880 (https://planetorbitrap.com/rawfilereader) and searched with SEQUEST [69] using an in-
881 house proteomic pipeline against a human protein target-decoy database containing both
882 SwissProt and TrEMBL entries (downloaded February 2014). The database was
883 concatenated onto a database of common contaminants (e.g. trypsin, human keratins).
884 Searches were performed with a 50 ppm precursor mass tolerance, 0.9 Da fragment
885 mass tolerance, trypsin digest with up to 2 missed cleavages. Allowed modifications
886 include cysteine carboxyamidomethylation (+57.02146), static TMT on lysine and peptide
887 N-temini (+229.16293) and up to 3 variable methionine oxidation (+15.99491). Peptide
888 spectral matches were filtered with a linear discriminant analysis (LDA) method to a 1%
889 FDR [61] and a protein-level FDR of 1% was also implemented [62]. For peptide
890 quantification, we extracted the TMT signal-to-noise and column normalized each
891 channel to correct for equal protein loading. Peptide spectral matches with summed
892 signal-to-noise less than 100 were excluded from final result. Lastly, each protein was
893 scaled such that the summed signal-to-noise for that protein across all channels equals
894 100, thereby generating a relative abundance (RA) measurement.
895
896 ***High content mitotic fraction assay***
897 Asynchronous hTERT RPE1-FUCCI wild-type or IRS2 KO cell lines were plated in a
898 black, clear-bottom 96-well plate (Corning, 3606). Plates were sealed with breathable
899 white rayon sealing tape (Nunc, 241205) to prevent evaporation following plating and

900 during all subsequent incubations. In experiments involving RNAi, cells were treated with
901 siRNAs for 24 hours. Cells were switched to fresh media, and compounds were added at
902 the indicated concentrations for an additional 18 hours. Following compound treatment,
903 cells were fixed and stained directly without additional washing steps (to avoid the loss of
904 loosely attached mitotic cells) with 10% formalin, 0.33 µg/mL Hoechst 33342, and 0.1%
905 Triton X-100 in DPBS. Plates were sealed with aluminum tape (Nunc, 276014) and were
906 incubated for 45 minutes room temperature in the dark before imaging. All experimental
907 conditions were represented in triplicate on the same plate. Plates were imaged using an
908 ImageXpress Micro high-content microscope (Molecular Devices) equipped with a 10x
909 objective lens. Four images were acquired per well, yielding a total of 12 images per
910 conditions. Images were processed automatically in ImageJ to identify and count nuclei
911 as well as measure their maximum fluorescence intensity. ImageJ output files were
912 pooled, and cumulative frequency curves for the maximum intensity of the cell population
913 in each condition were computed using MATLAB. An intensity threshold was set based
914 on the intensity of mitotic cells in control (DMSO-treated) wells to delineate interphase
915 cells from mitotic cells. The fraction of mitotic cells was calculated as the fraction of cells
916 above the set intensity threshold in MATLAB[17].
917
918 ***Materials Availability***
919 All mass spectrometry raw files will be available through the PRIDE archive upon
920 publication. All other data are available in the associated supplementary data files.
921 Further information and requests for resources and reagents should be directed to the
922 Lead Contact, Randy King (randy_king@hms.harvard.edu).
923
924 **Supplemental Information Legends**
925 ***Figure S1***: *Related to Figure 1*
926 (A) Asynchronous RPE1-FUCCI cells were treated with 1 µM palbociclib and imaged by
927 fluorescence time lapse microscopy for 20 hours. Frames at 0, 10, and 20 hours are
928 shown.
929 (B) From the experiment shown in Figure S1B, FITC intensity was quantified at 0 hours
930 (time of drug addition) and 20 hours. Each point represents the maximum FITC

931 intensity of an individual cell at the given time point. ns : not significant ; **** :
932 $p<0.0001$.
933 (C) Asynchronous RPE1-FUCCI cells were treated with 1 μM palbociclib for 20 hours.
934 Following G_1 arrest, cells were treated with either DMSO or APC/C inhibitors (6 μM
935 proTAME + 50 μM apcin) and imaged by fluorescence widefield time lapse microscopy
936 for an additional eight hours.
937 (D) Quantification of the experiment shown in S1D, as explained in S1B. Error bars = SD
938 among all of the cells quantified for each condition. ns: not significant ; **** : $p<0.0001$.
939 (E) RPE1-FUCCI cells were treated with 1 μM palbociclib for 20 hours. Following G_1
940 arrest, cells were either switched to fresh media containing no drug ("wash out"), fresh
941 media containing the same concentration of palbociclib ("palbociclib"), or fresh media
942 containing the same concentration of palbociclib and APC/C inhibitors (palbociclib +
943 APC/Ci). mAG1 intensity was quantified for all cells in a given frame every 2.7 hours
944 for 16 hours. Each data point represents the mean intensity ± SEM for at least 90 cells
945 from two different frames for each condition.
946
947 ***Figure S2***: *Related to Figure 2B*
948 (A) Asynchronous C_2C_{12} myoblasts and 3-day differentiated C_2C_{12} myotubes were lysed
949 and MyoD levels were measured by immunoblotting.
950 (B) Phase-contrast images of asynchronous (Day 0) C_2C_{12} myoblasts and 3-day
951 differentiated C_2C_{12} myotubes.
952 (C) Asynchronous C_2C_{12} myoblasts were transfected with a plasmid coding for the N-
953 terminal fragment of cyclin B1 (amino acids 1-88) fused to EGFP for 24 hours.
954 Following transfection, cells were switched to low-serum differentiation media
955 containing ITS for three days with media refreshment every 24 hours. After 3 days,
956 myotubes were acutely treated with either DMSO or APC/C inhibitors (6 μM proTAME
957 + 50 μM apcin) for an additional 8 hours. Myotubes were then harvested, and lysates
958 were analyzed for transgene expression by immunoblot.
959 (D) Asynchronous C_2C_{12} myoblasts were transfected with an siRNA directed against the
960 mouse Cdh1 sequence for 18 hours before being maintained in fresh media for an

961 additional 18 hours. Cells were harvested, and lysates were analyzed for the
962 expression of the indicated proteins.
963
964 ***Figure S3***: *Related to Figure 3*
965 HeLa cells were synchronized by double thymidine block and released into S-phase either
966 in the presence of DMSO or 5 μM RO3306. Cells were harvested at the indicated time
967 points for analysis of the given protein abundances and phosphorylation patterns in lysate
968 by immunoblot.
969
970 ***Figure S4***: *Related to Figure 4*
971 (A) (*top*) Asynchronous RPE1 cells expressing doxycycline-inducible, C-terminally HA
972 tagged IRS2 variants were treated with a dose range of doxycycline. HA and IRS2
973 expression levels were analyzed by immunoblotting cell lysates. Red = doxycycline
974 dose used for all experiments. (*bottom*) Asynchronous C_2C_{12} cells expressing
975 doxycycline-inducible, C-terminally HA tagged IRS2 variants were treated with a dose
976 range of doxycycline. HA and IRS2 expression levels were analyzed by
977 immunoblotting cell lysates. Red = doxycycline dose used for all experiments.
978 (B) (*left*) Asynchronous RPE1 cells expressing doxycycline-inducible, C-terminally HA-
979 tagged variants were lysed, and a dilution series of lysate was analyzed for HA
980 expression by immunoblot. The protein amount highlighted in red, 15 μg, was the
981 amount loaded for all immunoblot experiments. The corresponding Coomassie
982 stained gel is shown below. (*right*) Quantification of the experiment at left. Linear
983 regression calculations were made, and lines were plotted over data. For WT, R^2=
984 0.97. For DM, R^2=0.99
985 (C) *(left*) RPE1 cells stably expressing lentivirus generated, C-terminally HA-tagged IRS2
986 wild type (WT) and R972A (DM) constructs were arrested in G_1 with 1 μM palbociclib
987 for 20 hours. Cells were then acutely treated with either DMSO or the indicated dose
988 range of APC/C inhibitors for an additional 8 hours. Cells were then harvested, and
989 lysate was analyzed for HA expression by immunoblot. The lane denoted t_0 indicates
990 a sample that was collected at the time of drug addition. (*right*) Quantification of the

991 experiment at left. Plot shows HA intensity normalized to a loading control (either
992 GAPDH or Ponceau) and to the DMSO condition. Error bars = mean ± SEM.
993
994 ***Figure S5***: *Related to Figure 5*
995 (A) Hierarchical clustering for the nine conditions analyzed by TMT-coupled quantitative
996 mass spectrometry in wild type and ΔIRS2 cell lines.
997 (B) Venn diagrams depicting proteins that (*left*) decrease significantly >20% relative to
998 WT cells in both ΔIRS2 cell lines and (*right*) increase significantly >20% relative to WT
999 in both ΔIRS2 cell lines.
1000 (C) Gene ontology (GO) term enrichment of proteins that increase in both ΔIRS2 cell lines
1001 relative to WT cells.
1002 (D) Heat map for proteins in the "oxidation-reduction process" GO category increasing
1003 in both ΔIRS2 cell lines relative to WT cells.
1004
1005 ***Figure S6***: Related to Figure 5
1006 (E) Growth curves for IRS2 knockout cell lines.
1007 (F) Asynchronous RPE1 WT and IRS2 KO cells were imaged every five minutes by
1008 widefield time lapse microscopy for 36 hours. The fraction of cells that entered
1009 mitosis over this time span was measured manually, and cumulative frequency
1010 curves for mitotic entry were plotted. WT: n= 33 ; ΔIRS2-A: n=42; ΔIRS2-B: n=42.
1011 (G) Fractional abundance of cell-cycle related proteins shown in **Figure 5D-5E** depleted
1012 in ΔIRS2 cell lines relative to WT cells. ΔIRS2-A median abundance = 0.70 ; ΔIRS2-B
1013 median abundance = 0.66.
1014
1015 ***Figure S7***: *Related to Figure 6*
1016 (A) Representative frames from high-content nuclear imaging experiment for mitotic
1017 fraction based on DAPI intensity. Asynchronous RPE1 WT or IRS2 KO cell lines were
1018 treated with 900 nM nocodazole for 18 hours before fixing and DAPI staining.
1019 (B) Asynchronous RPE1 WT and IRS2 KO cell lines were imaged every five minutes by
1020 widefield time lapse microscopy for 36 hours. Each point represents an individual cell's
1021 mitotic duration, measured as the time from nuclear envelope breakdown (NEB) to

1022 division, slippage, or cell death. Error bars = mean ± SD. *p*-values were calculated
1023 using one-way ANOVA. ns = not statistically significant.
1024 (C) Asynchronous RPE1 WT and IRS2 KO cell lines were imaged as in (B). Images are
1025 representative of an unperturbed mitosis from NEB to cytokinesis for each cell line.
1026 Time (in minutes) in upper right corner indicates time since NEB.
1027
1028 ***Figure S8***: *Related to Figures 1-2*
1029 Extended immunoblots from Figures 1 and 2
1030
1031 ***Figure S9***: *Related to Figures 3*
1032 Extended immunoblots from Figure 3
1033
1034 ***Figure S10****: Related to Figures 4-5*
1035 Extended immunoblots from Figures 4 and 5
1036
1037 ***Table S1***: APC/C inhibition in G_1 proteomics
1038
1039 ***Table S2***: Reported APC/C substrates identified by proteomics
1040
1041 ***Table S3***: 204 protein subset
1042
1043 ***Table S4***: IRS2 knockout cell proteomics
1044
1045 **References**
1046
1047 1. Haeusler, R.A., T.E. McGraw, and D. Accili, *Biochemical and cellular properties of*
1048 *insulin receptor signalling.* Nature Reviews Molecular Cell Biology, 2017. **19**: p. 31.

1049 2. Copps, K.D. and M.F. White, *Regulation of insulin sensitivity by serine/threonine*
1050 *phosphorylation of insulin receptor substrate proteins IRS1 and IRS2.*
1051 Diabetologia, 2012. **55**(10): p. 2565-2582.

1052 3. Lavin, D.P., M.F. White, and D.P. Brazil, *IRS proteins and diabetic complications.*
1053 Diabetologia, 2016. **59**(11): p. 2280-2291.

1054 4. Bouzakri, K., et al., *siRNA-based gene silencing reveals specialized roles of IRS-*
1055 *1/Akt2 and IRS-2/Akt1 in glucose and lipid metabolism in human skeletal muscle.*
1056 Cell Metab, 2006. **4**(1): p. 89-96.

1057 5. Long, Y.C., et al., *Insulin receptor substrates Irs1 and Irs2 coordinate skeletal*
1058 *muscle growth and metabolism via the Akt and AMPK pathways.* Mol Cell Biol,
1059 2011. **31**(3): p. 430-41.

1060 6. Besse-Patin, A., et al., *PGC1A regulates the IRS1:IRS2 ratio during fasting to*
1061 *influence hepatic metabolism downstream of insulin.* Proc Natl Acad Sci U S A,
1062 2019. **116**(10): p. 4285-4290.

1063 7. Scheufele, F., et al., *Evidence for a regulatory role of Cullin-RING E3 ubiquitin*
1064 *ligase 7 in insulin signaling.* Cell Signal, 2014. **26**(2): p. 233-239.

1065 8. Xu, X., et al., *The CUL7 E3 ubiquitin ligase targets insulin receptor substrate 1 for*
1066 *ubiquitin-dependent degradation.* Mol Cell, 2008. **30**(4): p. 403-14.

1067 9. Nakao, R., et al., *Ubiquitin ligase Cbl-b is a negative regulator for insulin-like*
1068 *growth factor 1 signaling during muscle atrophy caused by unloading.* Mol Cell
1069 Biol, 2009. **29**(17): p. 4798-811.

1070 10. Shi, J., et al., *The SCF-Fbxo40 complex induces IRS1 ubiquitination in skeletal*
1071 *muscle, limiting IGF1 signaling.* Dev Cell, 2011. **21**(5): p. 835-47.

1072 11. Rui, L., et al., *SOCS-1 and SOCS-3 block insulin signaling by ubiquitin-mediated*
1073 *degradation of IRS1 and IRS2.* J Biol Chem, 2002. **277**(44): p. 42394-8.

1074 12. Yi, J.S., et al., *MG53-induced IRS-1 ubiquitination negatively regulates skeletal*
1075 *myogenesis and insulin signalling.* Nat Commun, 2013. **4**: p. 2354.

1076 13. Kubota, N., et al., *Dynamic functional relay between insulin receptor substrate 1*
1077 *and 2 in hepatic insulin signaling during fasting and feeding.* Cell Metab, 2008.
1078 **8**(1): p. 49-64.

1079 14. Alfieri, C., S. Zhang, and D. Barford, *Visualizing the complex functions and*
1080 *mechanisms of the anaphase promoting complex/cyclosome (APC/C).* Open Biol,
1081 2017. **7**(11).

1082 15. Chang, L. and D. Barford, *Insights into the anaphase-promoting complex: a*
1083 *molecular machine that regulates mitosis.* Curr Opin Struct Biol, 2014. **29**: p. 1-9.

1084 16. Davey, N.E. and D.O. Morgan, *Building a Regulatory Network with Short Linear*
1085 *Sequence Motifs: Lessons from the Degrons of the Anaphase-Promoting*
1086 *Complex.* Mol Cell, 2016. **64**(1): p. 12-23.

1087 17. Sackton, K.L., et al., *Synergistic blockade of mitotic exit by two chemical inhibitors*
1088 *of the APC/C.* Nature, 2014. **514**(7524): p. 646-9.

1089 18. Zeng, X., et al., *Pharmacologic inhibition of the anaphase-promoting complex*
1090 *induces a spindle checkpoint-dependent mitotic arrest in the absence of spindle*
1091 *damage.* Cancer Cell, 2010. **18**(4): p. 382-95.

1092 19. Connell-Crowley, L., J.W. Harper, and D.W. Goodrich, *Cyclin D1/Cdk4 regulates*
1093 *retinoblastoma protein-mediated cell cycle arrest by site-specific phosphorylation.*
1094 Mol Biol Cell, 1997. **8**(2): p. 287-301.

1095 20. Sakaue-Sawano, A., et al., *Visualizing spatiotemporal dynamics of multicellular*
1096 *cell-cycle progression.* Cell, 2008. **132**(3): p. 487-98.

1097 21. Prinz, S., et al., *The regulation of Cdc20 proteolysis reveals a role for the APC*
1098 *components Cdc23 and Cdc27 during S phase and early mitosis.* Current Biology,
1099 1998. **8**(13): p. 750-760.

1100 22. Puklowski, A., et al., *The SCF-FBXW5 E3-ubiquitin ligase is regulated by PLK4*
1101 *and targets HsSAS-6 to control centrosome duplication.* Nat Cell Biol, 2011. **13**(8):
1102 p. 1004-9.

1103 23. Klitzing, C., et al., *APC/C(Cdh1)-mediated degradation of the F-box protein NIPA*
1104 *is regulated by its association with Skp1.* PLoS One, 2011. **6**(12): p. e28998.

1105 24. Krystkowiak, I. and N.E. Davey, *SLiMSearch: a framework for proteome-wide*
1106 *discovery and annotation of functional modules in intrinsically disordered regions.*
1107 Nucleic Acids Res, 2017. **45**(W1): p. W464-W469.

1108 25. Zhao, W.M. and G. Fang, *Anillin is a substrate of anaphase-promoting*
1109 *complex/cyclosome (APC/C) that controls spatial contractility of myosin during late*
1110 *cytokinesis.* J Biol Chem, 2005. **280**(39): p. 33516-24.

1111 26. Ke, P.Y., et al., *Control of dTTP pool size by anaphase promoting*
1112 *complex/cyclosome is essential for the maintenance of genetic stability.* Genes
1113 Dev, 2005. **19**(16): p. 1920-33.

1114 27. Eguren, M., et al., *A synthetic lethal interaction between APC/C and*
1115 *topoisomerase poisons uncovered by proteomic screens.* Cell Rep, 2014. **6**(4): p.
1116 670-83.

1117 28. Kramer, E.R., et al., *Mitotic regulation of the APC activator proteins CDC20 and*
1118 *CDH1.* Mol Biol Cell, 2000. **11**(5): p. 1555-69.

1119 29. Chen, L., et al., *Plk1 phosphorylation of IRS2 prevents premature mitotic exit via*
1120 *AKT inactivation.* Biochemistry, 2015. **54**(15): p. 2473-80.

1121 30. Glotzer, M., A.W. Murray, and M.W. Kirschner, *Cyclin is degraded by the ubiquitin*
1122 *pathway.* Nature, 1991. **349**(6305): p. 132-8.

1123 31. Sun, X.J., et al., *Role of IRS-2 in insulin and cytokine signalling.* Nature, 1995.
1124 **377**(6545): p. 173-7.

1125 32. Clijsters, L., J. Ogink, and R. Wolthuis, *The spindle checkpoint, APC/C(Cdc20),*
1126 *and APC/C(Cdh1) play distinct roles in connecting mitosis to S phase.* J Cell Biol,
1127 2013. **201**(7): p. 1013-26.

1128 33. Brito, D.A. and C.L. Rieder, *Mitotic checkpoint slippage in humans occurs via cyclin*
1129 *B destruction in the presence of an active checkpoint.* Curr Biol, 2006. **16**(12): p.
1130 1194-200.

1131 34. Hornbeck, P.V., et al., *PhosphoSitePlus, 2014: mutations, PTMs and*
1132 *recalibrations.* Nucleic Acids Res, 2015. **43**(Database issue): p. D512-20.

1133 35. Wang, H., et al., *Pds1 phosphorylation in response to DNA damage is essential*
1134 *for its DNA damage checkpoint function.* Genes Dev, 2001. **15**(11): p. 1361-72.

1135 36. Mailand, N. and J.F. Diffley, *CDKs promote DNA replication origin licensing in*
1136 *human cells by protecting Cdc6 from APC/C-dependent proteolysis.* Cell, 2005.
1137 **122**(6): p. 915-26.

1138 37. Holt, L.J., *Regulatory modules: Coupling protein stability to phopshoregulation*
1139 *during cell division.* FEBS Lett, 2012. **586**(17): p. 2773-7.

1140 38. Chirivella, L., et al., *Cyclin-Dependent Kinase 4 Regulates Adult Neural Stem Cell*
1141 *Proliferation and Differentiation in Response to Insulin.* Stem Cells, 2017. **35**(12):
1142 p. 2403-2416.

1143 39. Wu, S., et al., *IRS-2, but not IRS-1, can sustain proliferation and rescue UBF*
1144 *stabilization in InR or InR defective signaling of 32D myeloid cells.* Cell Cycle,
1145 2009. **8**(19): p. 3218-26.

1146 40. Folli, F., et al., *Altered insulin receptor signalling and beta-cell cycle dynamics in*
1147 *type 2 diabetes mellitus.* PLoS One, 2011. **6**(11): p. e28050.

1148 41. Wan, Y., X. Liu, and M.W. Kirschner, *The Anaphase-Promoting Complex Mediates*
1149 *TGF-β Signaling by Targeting SnoN for Destruction.* Molecular Cell, 2001. **8**(5): p.
1150 1027-1039.

1151 42. Zhang, P.J., et al., *CUE domain containing 2 regulates degradation of*
1152 *progesterone receptor by ubiquitin-proteasome.* EMBO J, 2007. **26**(7): p. 1831-42.

1153 43. Song, M.S., et al., *Nuclear PTEN regulates the APC-CDH1 tumor-suppressive*
1154 *complex in a phosphatase-independent manner.* Cell, 2011. **144**(2): p. 187-99.

1155 44. Choi, B.H., et al., *Cdh1, a substrate-recruiting component of anaphase-promoting*
1156 *complex/cyclosome (APC/C) ubiquitin E3 ligase, specifically interacts with*
1157 *phosphatase and tensin homolog (PTEN) and promotes its removal from*
1158 *chromatin.* J Biol Chem, 2014. **289**(25): p. 17951-9.

1159 45. Choi, E., et al., *Mitotic regulators and the SHP2-MAPK pathway promote IR*
1160 *endocytosis and feedback regulation of insulin signaling.* Nature Communications,
1161 2019. **10**(1): p. 1473.

1162 46. Choi, E., et al., *Mitotic Checkpoint Regulators Control Insulin Signaling and*
1163 *Metabolic Homeostasis.* Cell, 2016. **166**(3): p. 567-581.

1164 47. Lei, L., et al., *IRS2 depletion inhibits cell proliferation and decreases hormone*
1165 *secretion in mouse granulosa cells.* J Reprod Dev, 2018. **64**(5): p. 409-416.

1166 48. Shirakawa, J., et al., *Insulin Signaling Regulates the FoxM1/PLK1/CENP-A*
1167 *Pathway to Promote Adaptive Pancreatic beta Cell Proliferation.* Cell Metab, 2017.
1168 **25**(4): p. 868-882 e5.

1169 49. Khumukcham, S.S., et al., *Hematopoietic PBX-interacting protein is a substrate*
1170 *and an inhibitor of the APC/C-Cdc20 complex and regulates mitosis by stabilizing*
1171 *cyclin B1.* J Biol Chem, 2019. **294**(26): p. 10236-10252.

1172 50. DeWard, A.D. and A.S. Alberts, *Ubiquitin-mediated degradation of the formin*
1173 *mDia2 upon completion of cell division.* J Biol Chem, 2009. **284**(30): p. 20061-9.

1174 51. Jeng, J.C., et al., *Cdh1 controls the stability of TACC3.* Cell Cycle, 2009. **8**(21): p.
1175 3537-44.

1176 52. Zhang, W.N., et al., *Phosphorylation-triggered CUEDC2 degradation promotes*
1177 *UV-induced G1 arrest through APC/C(Cdh1) regulation.* Proc Natl Acad Sci U S
1178 A, 2013. **110**(27): p. 11017-22.

1179 53. Singh, S.A., et al., *Co-regulation proteomics reveals substrates and mechanisms*
1180 *of APC/C-dependent degradation.* EMBO J, 2014. **33**(4): p. 385-99.

1181 54. Song, L. and M. Rape, *Regulated degradation of spindle assembly factors by the*
1182 *anaphase-promoting complex.* Mol Cell, 2010. **38**(3): p. 369-82.

1183 55. Seki, A. and G. Fang, *CKAP2 is a spindle-associated protein degraded by APC/C-*
1184 *Cdh1 during mitotic exit.* J Biol Chem, 2007. **282**(20): p. 15103-13.

1185 56. Drosopoulos, K., et al., *APC/C is an essential regulator of centrosome clustering.*
1186 Nat Commun, 2014. **5**: p. 3686.

1187 57. McGarry, T.J. and M.W. Kirschner, *Geminin, an Inhibitor of DNA Replication, Is*
1188 *Degraded during Mitosis.* Cell, 1998. **93**(6): p. 1043-1053.

1189 58. Choi, E., et al., *BubR1 acetylation at prometaphase is required for modulating*
1190 *APC/C activity and timing of mitosis.* EMBO J, 2009. **28**(14): p. 2077-89.

1191 59. Schneider, C.A., W.S. Rasband, and K.W. Eliceiri, *NIH Image to ImageJ: 25 years*
1192 *of image analysis.* Nature Methods, 2012. **9**(7): p. 671-675.

1193 60. Oegema, K., et al., *Functional analysis of a human homologue of the Drosophila*
1194 *actin binding protein anillin suggests a role in cytokinesis.* J Cell Biol, 2000. **150**(3):
1195 p. 539-52.

1196 61. Huttlin, E.L., et al., *A tissue-specific atlas of mouse protein phosphorylation and*
1197 *expression.* Cell, 2010. **143**(7): p. 1174-89.

1198 62. Savitski, M.M., et al., *A Scalable Approach for Protein False Discovery Rate*
1199 *Estimation in Large Proteomic Data Sets.* Mol Cell Proteomics, 2015. **14**(9): p.
1200 2394-404.

1201 63. Carbon, S., et al., *AmiGO: online access to ontology and annotation data.*
1202 Bioinformatics, 2009. **25**(2): p. 288-9.

1203 64. Navarrete-Perea, J., et al., *Streamlined Tandem Mass Tag (SL-TMT) Protocol: An*
1204 *Efficient Strategy for Quantitative (Phospho)proteome Profiling Using Tandem*
1205 *Mass Tag-Synchronous Precursor Selection-MS3.* J Proteome Res, 2018. **17**(6):
1206 p. 2226-2236.

1207 65. McAlister, G.C., et al., *MultiNotch MS3 enables accurate, sensitive, and*
1208 *multiplexed detection of differential expression across cancer cell line proteomes.*
1209 Anal Chem, 2014. **86**(14): p. 7150-8.

1210 66. Schweppe, D.K., et al., 2019.

1211 67. Erickson, B.K., et al., *Active Instrument Engagement Combined with a Real-Time*
1212 *Database Search for Improved Performance of Sample Multiplexing Workflows.* J
1213 Proteome Res, 2019. **18**(3): p. 1299-1306.

1214 68. Perez-Riverol, Y., et al., *The PRIDE database and related tools and resources in*
1215 *2019: improving support for quantification data.* Nucleic Acids Res, 2019. **47**(D1):
1216 p. D442-D450.

1217 69. Eng, J., A. McCormack, and J. Yates, *An approach to correlate tandem mass*
1218 *spectral data of peptides with amino acid sequences in a protein database.* J Am
1219 Soc Mass Spectrom, 1994. **5**(11): p. 976-989.
1220

Figure 1

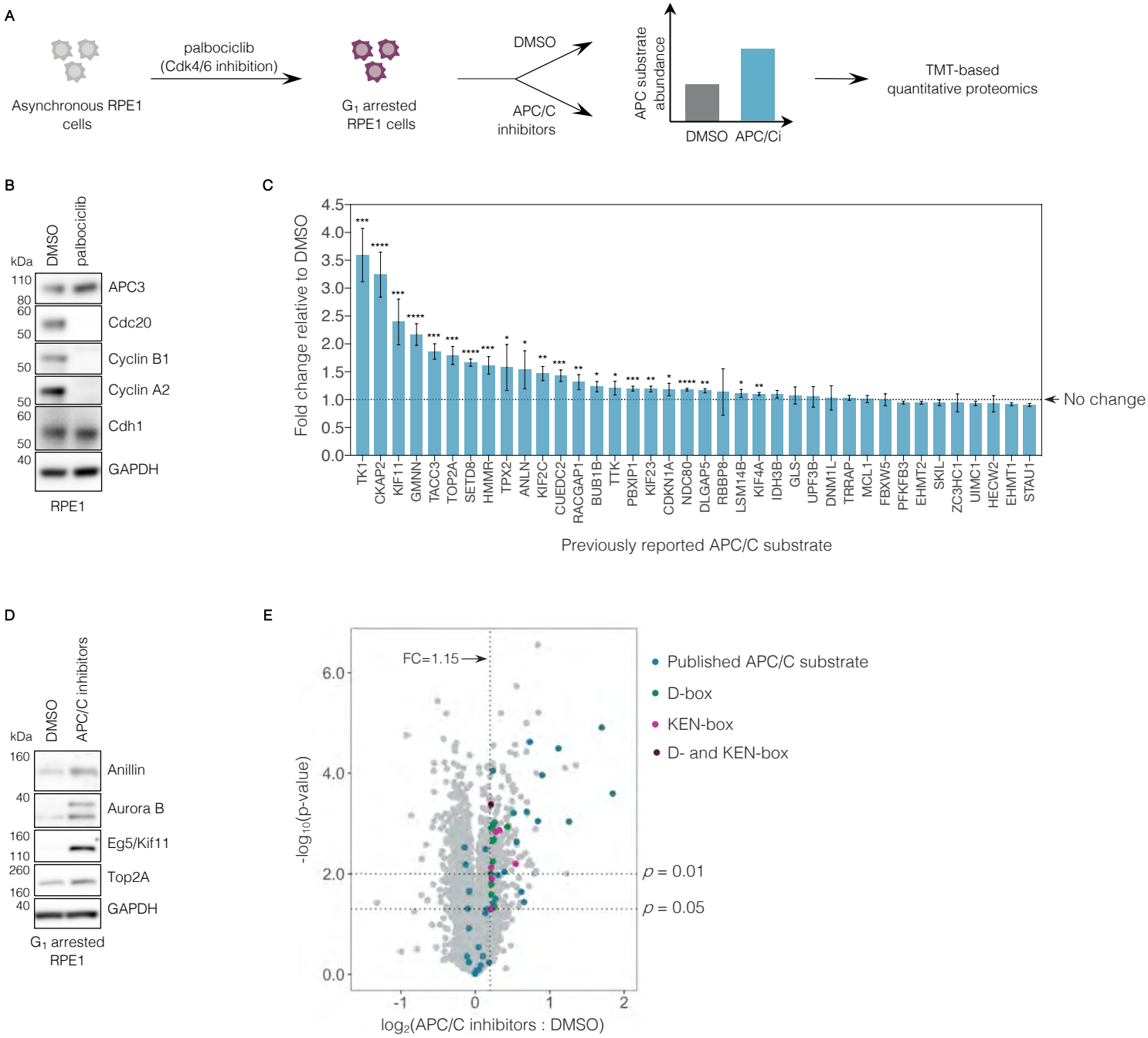
A
Asynchronous RPE1 cells
palbociclib (Cdk4/6 inhibition)
G1 arrested RPE1 cells
DMSO
APC/C inhibitors
APC substrate abundance
DMSO
APC/Ci
TMT-based quantitative proteomics
B
kDa
DMSO
palbociclib
APC3
Cdc20
Cyclin B1
Cyclin A2
Cdh1
GAPDH
RPE1
C
Fold change relative to DMSO
No change
Previously reported APC/C substrate
D
kDa
DMSO
APC/C inhibitors
Anillin
Aurora B
Eg5/Kif11
Top2A
GAPDH
G1 arrested RPE1
E
FC=1.15
p = 0.01
p = 0.05
Published APC/C substrate
D-box
KEN-box
D- and KEN-box
-log10(p-value)
log2(APC/C inhibitors : DMSO)

Figure 2

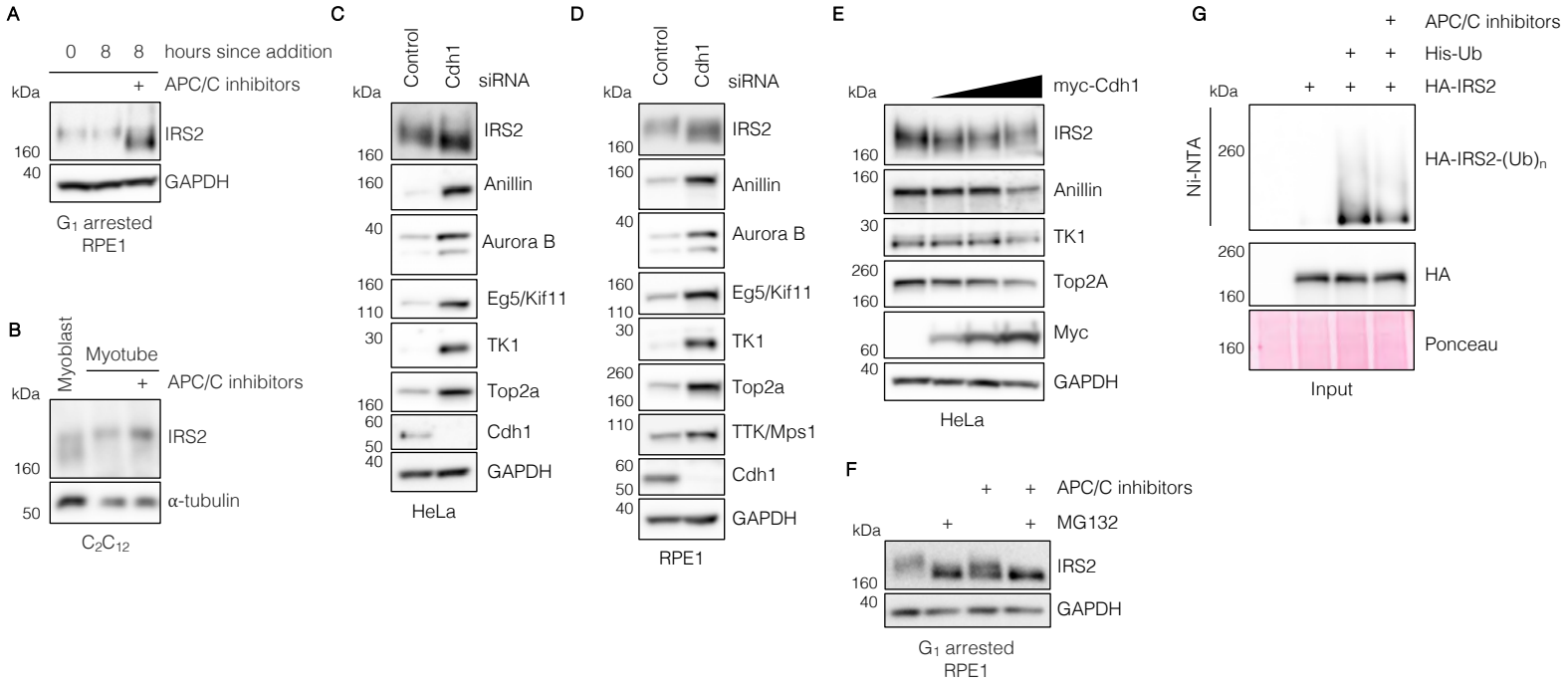
A
0 8 8 hours since addition
+ APC/C inhibitors
kDa
160
40
IRS2
GAPDH
G1 arrested RPE1
B
Myoblast
Myotube
+ APC/C inhibitors
kDa
160
50
IRS2
α-tubulin
C2C12
C
Control
Cdh1
siRNA
kDa
160
160
40
160
110
30
160
60
50
40
IRS2
Anillin
Aurora B
Eg5/Kif11
TK1
Top2a
Cdh1
GAPDH
HeLa
D
Control
Cdh1
siRNA
kDa
160
160
40
160
110
30
260
160
110
60
50
40
IRS2
Anillin
Aurora B
Eg5/Kif11
TK1
Top2a
TTK/Mps1
Cdh1
GAPDH
RPE1
E
kDa
myc-Cdh1
160
160
30
260
160
60
40
IRS2
Anillin
TK1
Top2A
Myc
GAPDH
HeLa
F
+ + APC/C inhibitors
+ + MG132
kDa
160
40
IRS2
GAPDH
G1 arrested RPE1
G
+ APC/C inhibitors
+ + His-Ub
+ + + HA-IRS2
kDa
Ni-NTA
260
HA-IRS2-(Ub)n
260
160
HA
160
Ponceau
Input

Figure 3

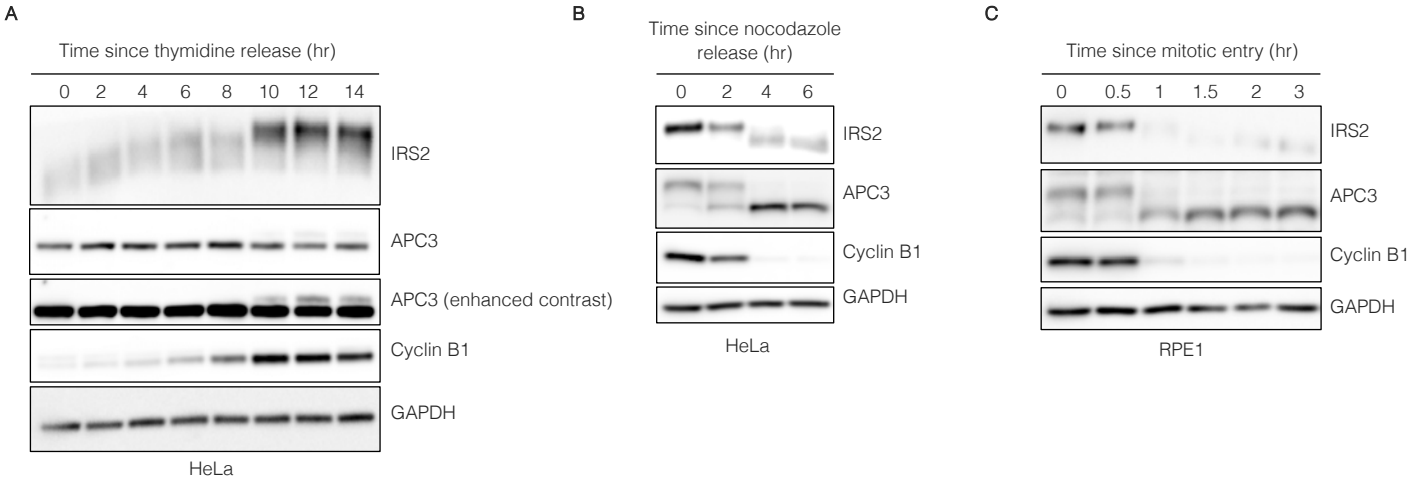
A
Time since thymidine release (hr)
0 2 4 6 8 10 12 14
IRS2
APC3
APC3 (enhanced contrast)
Cyclin B1
GAPDH
HeLa
B
Time since nocodazole release (hr)
0 2 4 6
IRS2
APC3
Cyclin B1
GAPDH
HeLa
C
Time since mitotic entry (hr)
0 0.5 1 1.5 2 3
IRS2
APC3
Cyclin B1
GAPDH
RPE1

Figure 4

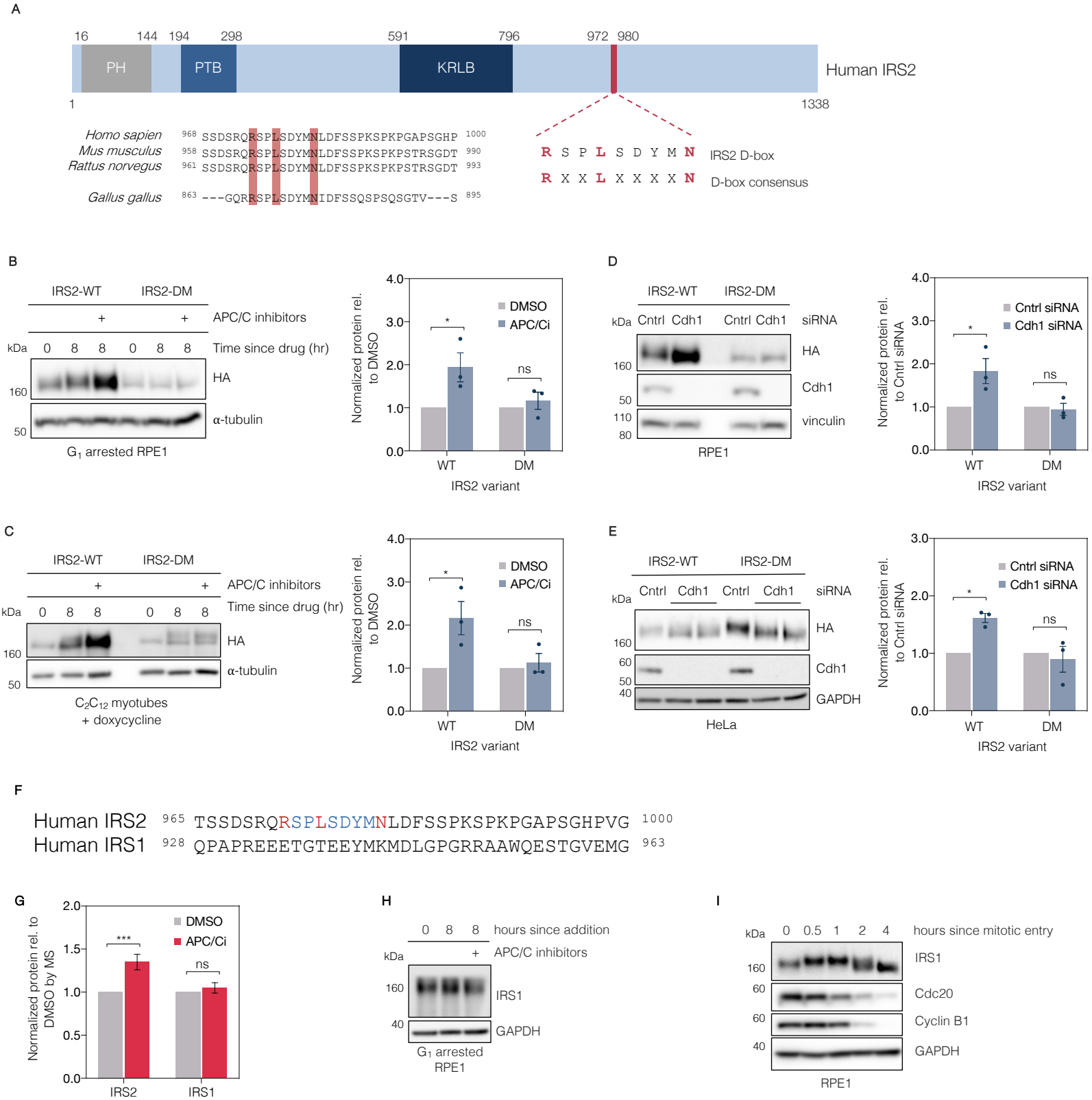
A
16
144
194
298
591
796
972
980
PH
PTB
KRLB
Human IRS2
1
1338
Homo sapien 968 SSDSRQRSPLSDYMNLDFSSPKSPKPGAPSGHP 1000
Mus musculus 958 SSDSRQRSPLSDYMNLDFSSPKSPKPSTRSGDT 990
Rattus norvegus 961 SSDSRQRSPLSDYMNLDFSSPKSPKPSTRSGDT 993
Gallus gallus 863 ---GQRRSPLSDYMNIDFSSQSPSQSGTV---S 895
R S P L S D Y M N IRS2 D-box
R X X L X X X X N D-box consensus
B
IRS2-WT
IRS2-DM
APC/C inhibitors
Time since drug (hr)
kDa
HA
α-tubulin
G1 arrested RPE1
Normalized protein rel. to DMSO
DMSO
APC/Ci
ns
WT
DM
IRS2 variant
C
C2C12 myotubes + doxycycline
D
Cntrl
Cdh1
siRNA
vinculin
RPE1
Cntrl siRNA
Cdh1 siRNA
Normalized protein rel. to Cntrl siRNA
E
GAPDH
HeLa
F
Human IRS2 965 TSSDSRQRSPLSDYMNLDFSSPKSPKPGAPSGHPVG 1000
Human IRS1 928 QPAPREEETGTEEYMKMDLGPGRRAAWQESTGVEMG 963
G
Normalized protein rel. to DMSO by MS
IRS2
IRS1
H
hours since addition
IRS1
GAPDH
G1 arrested RPE1
I
hours since mitotic entry
Cdc20
Cyclin B1
RPE1

Figure 5

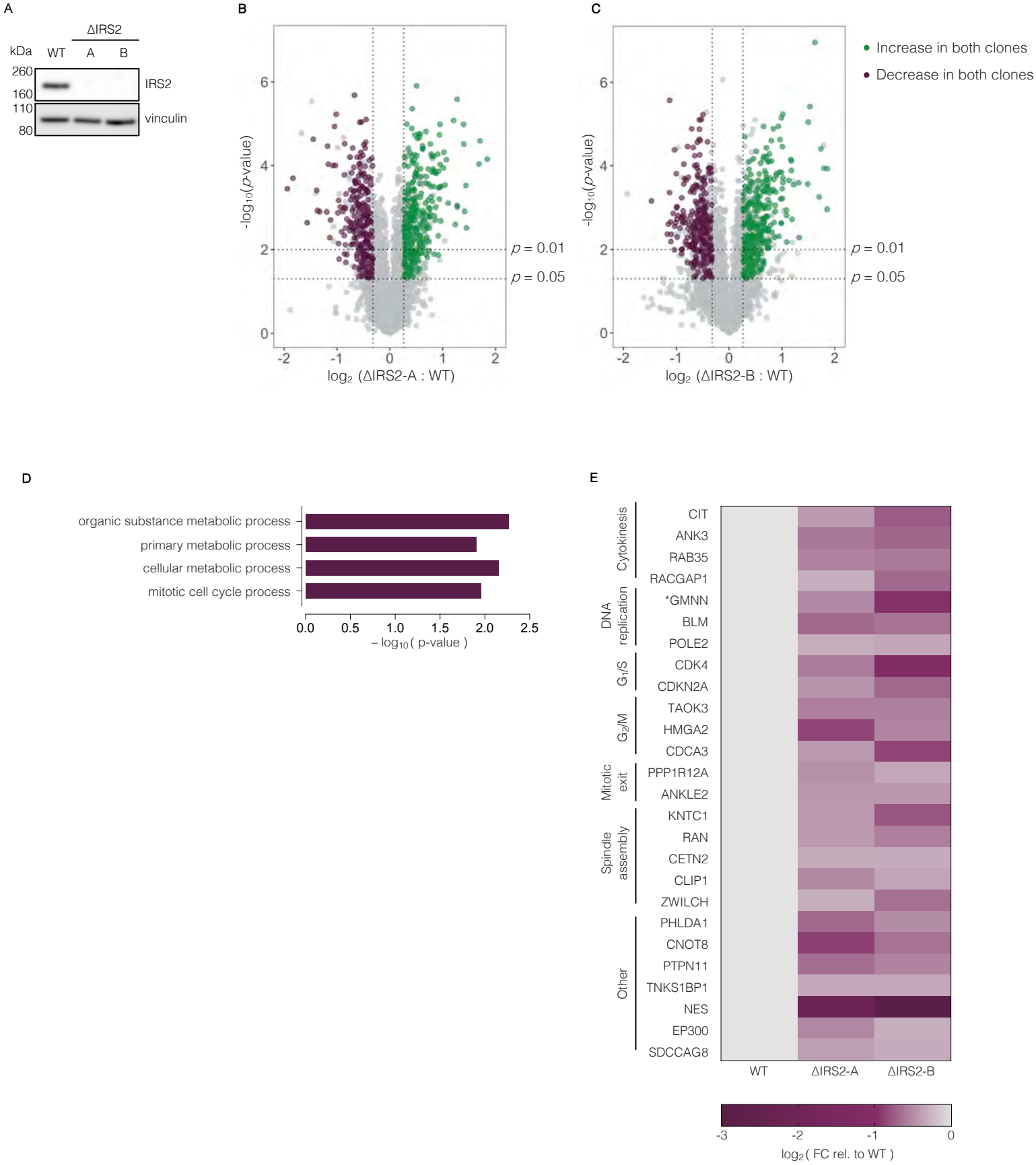
A
ΔIRS2
kDa
WT
A
B
260
160
110
80
IRS2
vinculin
B
-log10(p-value)
p = 0.01
p = 0.05
log2 (ΔIRS2-A : WT)
C
Increase in both clones
Decrease in both clones
log2 (ΔIRS2-B : WT)
D
organic substance metabolic process
primary metabolic process
cellular metabolic process
mitotic cell cycle process
– log10(p-value)
E
Cytokinesis
DNA replication
G1/S
G2/M
Mitotic exit
Spindle assembly
Other
CIT
ANK3
RAB35
RACGAP1
*GMNN
BLM
POLE2
CDK4
CDKN2A
TAOK3
HMGA2
CDCA3
PPP1R12A
ANKLE2
KNTC1
RAN
CETN2
CLIP1
ZWILCH
PHLDA1
CNOT8
PTPN11
TNKS1BP1
NES
EP300
SDCCAG8
WT
ΔIRS2-A
ΔIRS2-B
log2(FC rel. to WT)

Figure 6

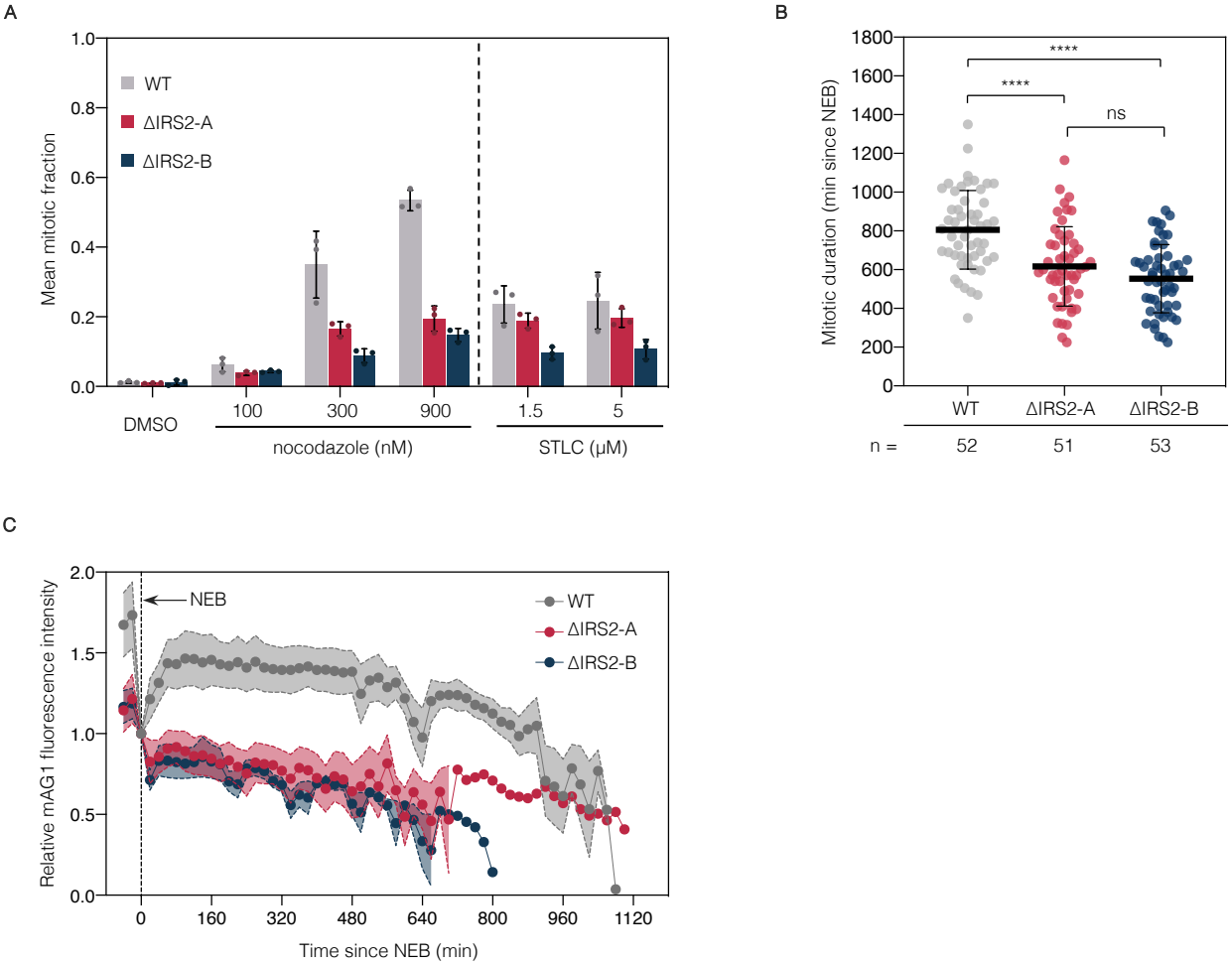
A
Mean mitotic fraction
WT
ΔIRS2-A
ΔIRS2-B
DMSO
100
300
900
1.5
5
nocodazole (nM)
STLC (μM)
B
Mitotic duration (min since NEB)
****
****
ns
WT
ΔIRS2-A
ΔIRS2-B
n =
52
51
53
C
Relative mAG1 fluorescence intensity
NEB
WT
ΔIRS2-A
ΔIRS2-B
Time since NEB (min)

Figure 7

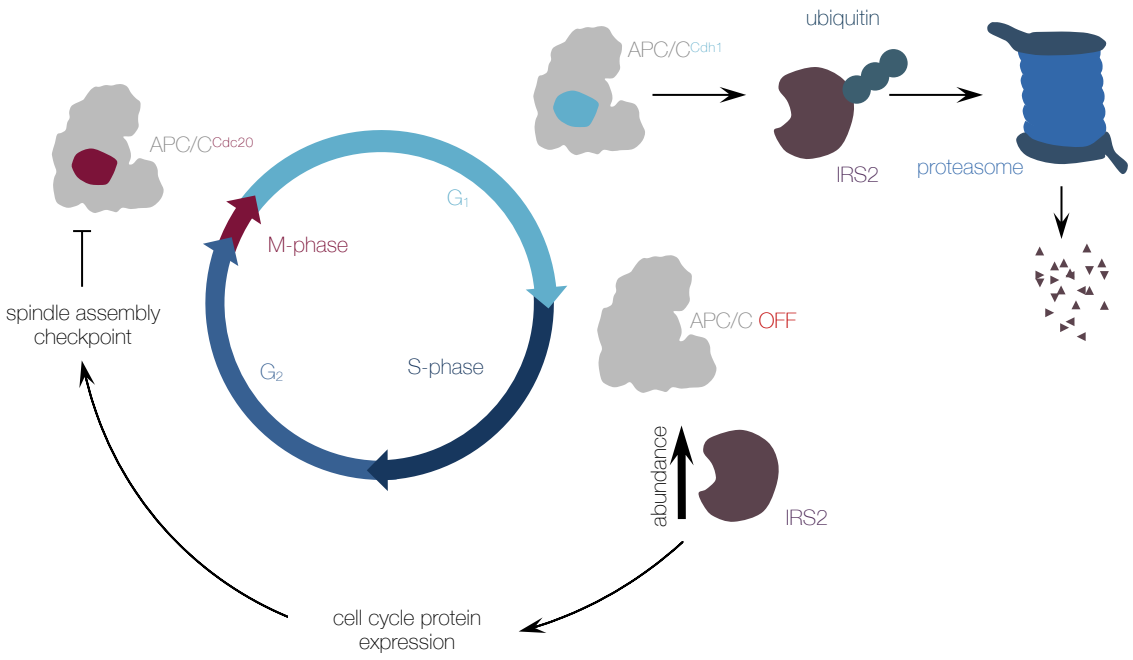
APC/C^{Cdc20}
spindle assembly checkpoint
M-phase
G_1
S-phase
G_2
APC/C^{Cdh1}
ubiquitin
IRS2
proteasome
APC/C OFF
abundance
IRS2
cell cycle protein expression